Ultrafast Carrier Dynamics of Laser-ablated Graphite and Reduced Graphene Oxide with Metal Composites

September 2019

Tokushima University
Graduate School of Advanced Technology and Science
Systems Innovation Engineering, Optical Systems Engineering
Doctoral Course

YATIN MADHUKAR BHAMARE

Abstract

Carbon based materials are considered as a rewarding contestant for optical devices due to its novel properties. Graphite is a most stable allotrope of carbon with a layered and planar structure. Graphene is the two-dimensional lattice of carbon atoms in a honeycomb arrangement, and is attracting significant attention from the scientific community. There was a rapid growth of graphene-based two-dimensional counterparts, the most famous among which is reduced graphene oxide (rGO).

In this study, graphite is laser-ablated and different analytical methods such as XRD and Raman spectroscopy are used to evaluate the crystalline nature. Reduced graphene oxide is prepared by using modified Hummers method and reduced it by thermal reduction method. It is decorated with Au, Pd and Pt nanoparticles by chemical synthesis. In XRD, it indicates the decreased intensity after laser ablation but no change in peak positions resulted as graphite is very strong and hard material. Raman spectroscopy indicates, after laser ablation, D-band and G´-band peaks are slightly shifted to larger wave number side by 5-10 wave numbers, but there is no obvious change in peak position for G-band. Also, the G/D ratio decreases from 4.13 to 3.38, indicating the edge effect in laser ablated nanostructures. UV-Vis spectra confirmed the peaks of both graphite (non-ablated and laser-ablated) and rGO at 274 nm and 267 nm, respectively. It also confirms the synthesis of rGO with Au, Pd and Pt composites successfully. Scanning electron microscopy (SEM) used to evaluate structural characteristics shows the overlapping layered structure after ablation. It also reveals the layered structure of rGO with successful composition of Au, Pd and Pt nanoparticles. Photocatalysis activity of rGO with Au, Pd and Pt was observed using UV-Vis spectroscopy. rGO-Au shows faster degradation of methylene blue using both xenon white lamp and blue LED.

To study the ultrafast carrier dynamics, femtosecond transient absorption spectroscopy was used. Graphite, laser-ablated graphite and rGO shows carrier relaxation between 260 and 309 fs even after laser ablation damage, which is useful for future application of optical switching under high laser repetition. rGO with Au, Pd and Pt shows carrier relaxation between 177 and 304 fs with long lived component in ultrafast carrier dynamics. Surface plasmon resonance absorption and inter-band excitation of Au nanoparticle shows rGO-Au is useful composition for photocatalysis activity.

Acknowledgments

I would like to express my sincere gratitude to my PhD Supervisor, Professor Akihiro Furube, for his insightful guidance, visionary advices and genuine support in my PhD program. He is the kind of professor everyone in graduate school should want to have as a supervisor. He is extremely calm, patient and an excellent teacher. I feel very lucky to have a supervisor like him. Thank you so much…sensei!

Special thanks to my co-supervisor, Associate professor Pankaj Koinkar, without him my dream of PhD in Japan would not have been possible. He helped me from the beginning of the registration to my PhD program. I am very thankful to him for continuous encouragement, helpful discussions and research advises. I would like to thank M. A. More sir, for great collaboration and continuous support to my research experiments. Thanks to shin-ichiro Yanagiya for his helpful suggestions about my research. I am grateful to Satoshi Sugano for his technical support.

I would like to thank my parents, Sharmila and Madhukar Bhamare, for their understanding of my PhD study in Japan. Thank you so much for your financial support, encouragement and patience. Thanks to my brother Ketan, for always being my back bone. Thanks to my sister-in-law Priyanka, for always being my motivator. Special thanks to my niece Lavanya, for making me joyful by talking on video calls.

I would like to thank my labmates, Makato Kanazawa, Masahiro Okazaki, Atsushi Yamaguchi and Tomoya Ohara for making me comfortable in Japanese research culture, helping in daily life activities and exploring in Japan. Thanks to my Indian friends Krunal Girase, Mahesh Patil and Sidhhant Dhondage for making my life comfortable in Japan. I really appreciate the kindness, help and Indian dinners offered by Aparna Koinkar mam. It was always a joyful experience with Prapti and Arvin, whenever I visited to your house. Thanks to all my past and present labmates, Japanese friends and Foreign friends for making my life in Japan colorful and comfortable.

Dedicated to my all well-wishers on the earth

Contents

List of Figures

List of Tables

List of Schemes

Abbreviations

GO	Graphene oxide
rGO	Reduced Graphene Oxide
UV-Vis	Ultraviolet-visible
SEM	Scanning Electron Microscopy
XRD	X-Ray Diffraction
fs	Femtosecond
TAS	Transient Absorption Spectroscopy
Au	Gold
Pd	Palladium
Pt	Platinum
NP	Nanoparticle
GSB	Ground State Bleaching
SE	Stimulated Emission
IA	Induced Absorption
Nd:YAG	Neodymium-doped Yttrium Aluminum Garnet
MB	Methylene Blue
SPR	Surface Plasmon Resonance
FWHM	Full Width Half Maximum
LED	Light Emitting Diode

Chapter 1. An Overview of Graphite and rGO

1. Nanomaterials

Nanomaterials have made significant contribution to enhance the developments in nanoscience and nanotechnology. Especially, the development of nanomaterials with feature size of few nm size leads to specific applications in field of nanotechnology. Different type of nanomaterials, with feature size less than 100 nm, can be used in nanotechnology such as flash memory chips, sensors, electro optics devices and so on. Many efforts have been made to fulfil the growing demand of nanomaterials with feature size less than 50 nm which can be used for commercial applications. Keeping this in mind, it is essential to understand basic properties of nanomaterials at nanoscale level. At the same time, growing need to design and develop the simple method have been projected to cover synthesis and measure of nanomaterials. During the last two decades, researcher have used different approaches to significant progress have been made to understand basic phenomenon and properties of nanomaterials at nanoscale level. In this context, researchers from all over the world have widely explored various nanomaterials due to their outstanding physico-chemical properties suitable for technological applications.

Nanomaterials exhibit interesting and unique properties which is consider as an important consideration for technological application in the field of photonics, energy conversion, optical switching, display, sensors and optoelectronic devices. The promising technological applications are based on the basic principle, physical phenomenon, and related concepts of physics, chemistry, biology, and engineering. Thus, it is equally important to understand the basic phenomenon and optical properties of nanomaterials using appropriate spectroscopic techniques.

It is reported that the optical properties can be altered using visual features such as size, shape and bulk surface conditioning like irradiation, implantation, doping, and so on. Doping is considered as one of surface conditioning method which greatly affect to tailor the optical, electrical, magnetic of semiconductors and insulators.

2. Graphite

2.1 Introduction

Roman name charcoal and origin name “carbo” from Latin is now a days called as a ***carbon***. In modern world, carbon is the most beneficial and profitable element for various applications and markets. In the different sections of the industries, processing techniques of the carbon are well-established for various applications. Structure of the carbon reveals different properties as it is a well knows allotropic material. Diamond is the purest and expensive form of the carbon, until now it is the hardest material in the world. ***Graphite*** is the another form of carbon, it is a very soft material and has a grey color. In plane direction it is characterized as a good conductor. Carbon fibers and glassy carbon are the other form of carbon. Difference in the varying arrangements of their atomic structure classifies the material, otherwise these materials are made of the same carbon atoms [1].

Graphite is useful in the thermal management materials due to its low coefficient of thermal expansion, high thermal conductivity, low density and more important its low cost. In the following section, the properties of graphite are discussed in details.

2.2 Graphite structure

Graphite is naturally occurring in the form of flakes or lumps; it is rarely found in the form monocrystals. Graphite is an allotrope of element carbon which consists of layers of hexagonally arranged carbon atoms in a planer condensed ring system. A typical crystal structure of hexagonal graphite is shown in figure 1 where multiple graphene layers linked with triangular planar bonding and circle represent the position of each carbon atom.

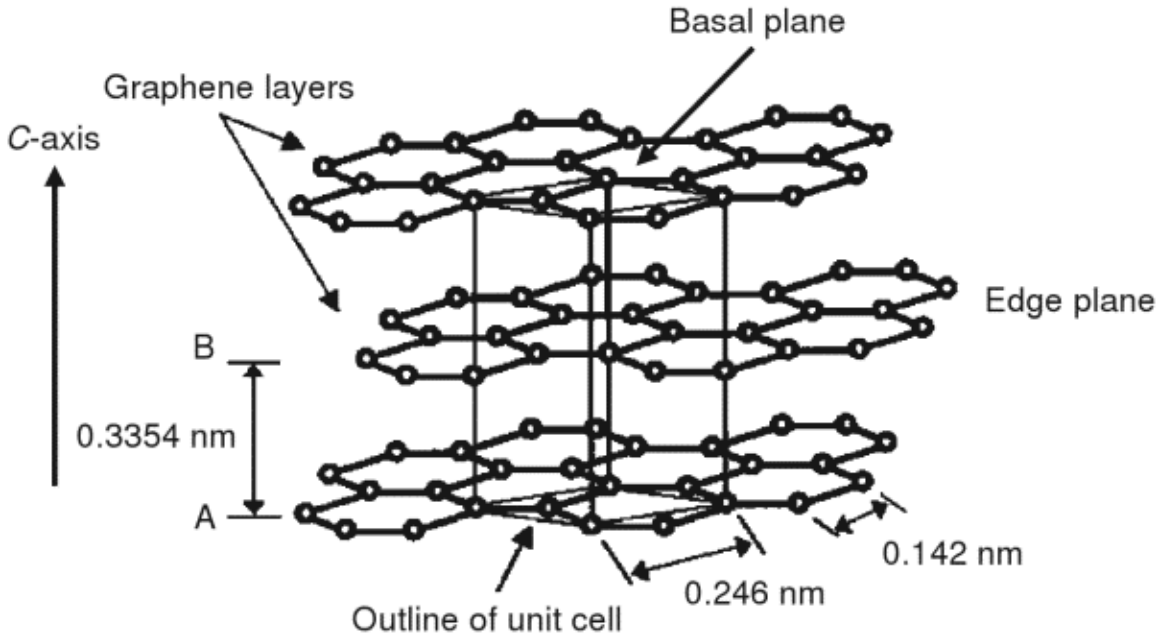

Figure 1. Crystal structure of hexagonal graphite, with triangular planar bonding within the graphene layers. [2]

Graphite contains hexagonal structure with many flat layers called as a ***graphene sheets.*** Low friction sliding of the planes between these graphene sheets are occurs, because these sheets are bonded to each other by weak Van der Waals forces. This effect determines the and self-lubricating property and high softness of the graphite.

Carbon atoms in each graphene layer are covalently bonded to three other atoms in the plane with the optimal bond of 120°. The outermost electron shell of carbon atom consists of four valence electrons, out of these only three electrons are used to form the covalent bonds. The fourth valence electron which do not have active participation in band formation, can be free electron and can easily move from outermost shell electron by an electric field. These electrons provide the electrical conductivity of graphite.

In graphite crystals, hexagonal graphite is the most common stacking sequence [1]. Crystal structure of graphite showing ABAB stacking sequence is shown in figure 2. Above

2200 °C temperature, the graphitization process of carbon is started and the well aligned structure is created.

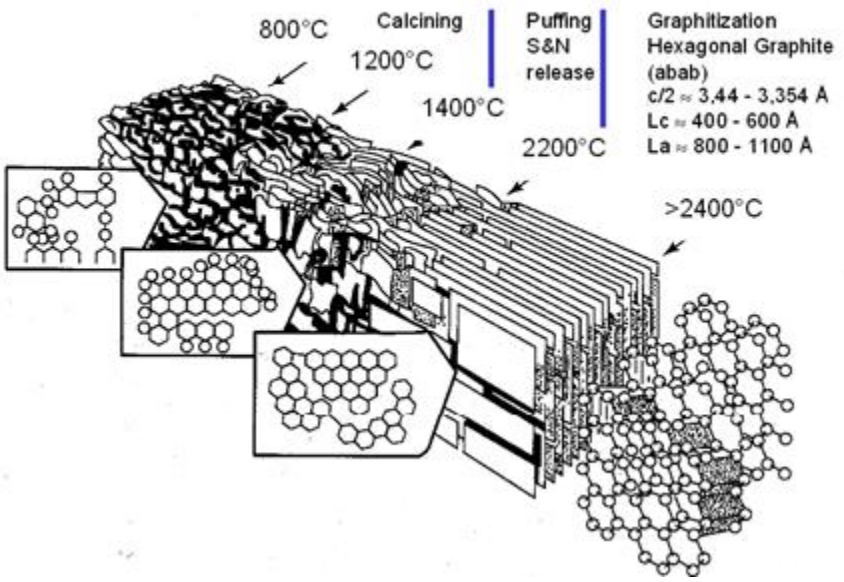

Figure 2. Crystal structure of graphite showing ABAB stacking sequence and unit cell. [2]

Difference between graphitized and non-graphitized carbon is shown in Figure 3. Graphitized carbon (a) is characterized by well aligned sheets which shows excellent thermal and electrical conductivity while non-graphitized carbon (b) is irregularly spread which decreases its work ability in the thermal applications.

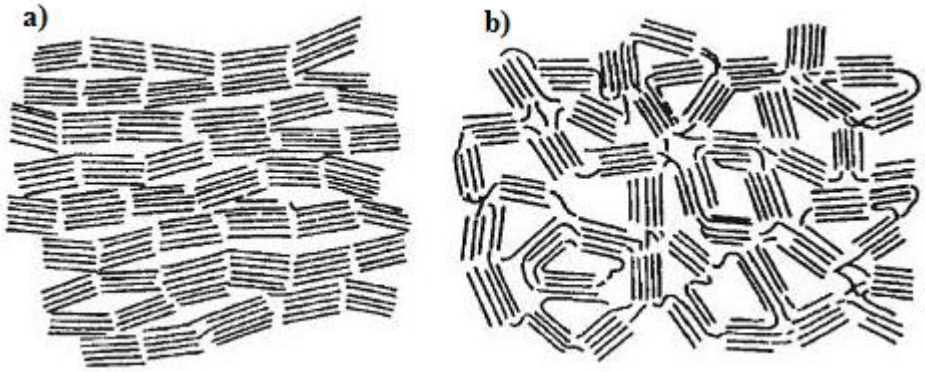

Figure 3. Differences between a) graphitize, b) and non-graphitize carbon. [2]

2.3 Physical properties of graphite

Considerable anisotropy of the material leads in the special crystal structure of graphite. It shows that the material has different properties when measured along ab directions within the plane or the c direction perpendicular to the planes. Following of the characteristic physical properties of graphite:

• Density is lower than diamond, this is because of the relatively large amount of space that is "wasted" between the sheets.

• High thermal stability (up to 4000K no degradation or phase changes).

• Softness and slipperiness, e.g. in pencils and as a dry lubricant (used in pencils, graphite sheets are rubbed off and stick to the paper).

• Insolubility in water and organic solvents. Reactions between solvent molecules and carbon atoms will never be strong enough to overcome the strong covalent bonds in graphite.

• Electrical conductivity. In the sheets, the delocalized electrons are free to move.

Table 1 summarizes the most notable physical properties of graphite.

Table 1. Physical properties of graphite [1]

Crystalline form	Hexagonal
Lattice parameters	a_0=0,246 nm, c_0 = 0.671 nm
Color	black
Theoretical Density	2.25 g/cm^3
Atomic volume	5.315 cm^3/mol
Sublimation point at 1 atm (estimated)	4000 K
Triple point (estimated)	4200 K
Boiling point (estimated)	4560 K
Heat of fusion	46.84 kJ/mol
Pauling electronegativity	2,5

2.4 Thermal properties of graphite

Thermal conductivity

As discussed in Section 2.2, the superior structure of graphite is validated as an excellent heat conductor (along in-plane direction). In the non-metals like graphite, heat conductivity is basically possible due to lattice vibrations. In stress annealed pyrolytic graphite, the thermal conductivity of a graphite crystal can be as high as 4180 W/(mK) in the ab directions for high crystallinity. However, around 390 W/(mK) in ab directions and 2 W/(mK) in c direction, the average value for commercial pyrolytic graphite is much lower. With temperature, the thermal conductivity of graphite decreases [1].

Specific heat

The specific heat of graphite is 8.033 – 8.635 J/mol*K at 25°C and increases with the given relationship:

(Specific heat: Amount of heat per mass unit required to raise the temperature by 1°C)

$$Cp=4.03+(1.14 * 10^{-3})\, T - [(2.04 * 105) / T^2]$$

Scheme 1. Relationship of specific heat to the temperature (T in degree K). [1]

Coefficient of thermal expansion

Coefficient of thermal expansion (CTE) is defined as the extent to which a material expands upon heating, it is the another important property of graphite. Between the carbon atoms of graphite, the interatomic spacing is a function of temperature. These atoms have their lowest energy position at 0 K. The temperature rises, when the energy increases. As a results, the atoms move further apart and start to vibrate. During the outward motion of the atoms the atomic bonds are not overstretched in the strongly bonded graphite (in the ab directions), the amplitude of vibration is also small. As a result, the dimensional changes remain small. When the atomic bond is weak like in the c direction, the dimensional changes and vibration amplitude are large. Thus, the thermal expansion factor of a graphite crystal is different (in two considered directions).

CTE increase with temperature is not linear (in c direction), it increases gradually and slowly. At 0°C the coefficient of thermal expansion is about $25x10^{-6}K^{-1}$ and about 400°C it can be reach $28x10^{-6}K^{-1}$. The thermal expansion in the ab direction is actually negative ($-0.5\ 10^{-6}K^{-1}$) up to approx. 400°C with a minimum at 0°C. It is possible that the observed negative expansion is due to the internal stress (called as poison effect) associated with the large expansion (in the c direction). The large thermal expansion anisotropy often results in structural problems and large internal stresses such as delamination between planes [1].

2.5 Electrical properties of graphite

Graphite is a non-metal; then also electrical conductivity is another characteristic property. Electrons are strongly bonded to the nucleus and are not free to move, in electrical insulators. Graphite is also considered as a semi-metal, it means that is an insulator normal to the basal plane and conductor in the basal plane. In the outermost electron shell, carbon has four valence electrons, from that three of them are used for the covalent bonds and the forth one is easily displaced from the electron shell by an electric field, therefore electrical conductivity is possible. These electrons provide the electrical conductivity of graphite. The spacing between planes is large and it is difficult for the electrons to move from one plane to another, in the c direction. Therefore, in that direction electrical conductivity is low [1].

2.6 Mechanical properties of graphite

Graphite can be found in automobiles, aircrafts or even golf club shafts, in spite of its high mineral softness, is used to produce high-strength, low weight composite materials. When the graphite sheets are rolled up into fibers, and then twisted into threads, along the fiber axis it is possible to take advantage of graphite strengths along the fiber axis. It is possible due to the sapient usage of the highly-oriented graphite in hexagonal planes. An epoxy resin, which provides a stable connection between the threads, these threads are then molded into a rolled shape and embedded inside a binder. The resulting composites have some of the highest strength-to-weight ratios of any materials excluding carbon nanotubes and diamond crystals. The bond between the atoms in the basal plane of a graphite crystal is significantly stronger than the bond between the planes in graphite.

3. Graphene, graphene oxide (GO) and reduced graphene oxide (rGO)

3.1 Introduction

This section describes carbon compound earlier known as s graphitic acid or graphite oxide (GO), and nowadays called as ***graphene oxide (GO)***. GO is considered as two-dimensional carbon sheet having many reactive oxygen containing functional groups attached to the basal plane. The thickness of each sheet is about 1 nm with lateral size ranges from a few nanometers and several microns. In the year1859, the first attempt to prepare GO in the laboratory was made by the scientist B. C. Brodie. However, it become more popular among the researchers in last decade due to its unique and outstanding properties. Many researchers attracted towards groundbreaking research on new material called as **graphene,** made up of single atomic layer of graphite which is discovered by two scientists Andre Geim and Konstantin Novoselov. This British duo received Nobel Prize in Physics in 2010 for their significant contribution on groundbreaking research on graphene. A number of different type of methods have been employed to prepare graphene by reducing GO. This section is primarily devoted to the structure, properties and synthesis route used prepare GO and rGO. Although graphene is most famous and popular material among researchers, GO is also equally important and has its own significance because of technological applications. GO is formed by oxidized carbon which is used as base materials for the preparation of various composites, alloys and derivatives.

Atomically thin layered materials called as two dimensional (2D) nanomaterials, for example graphene, tungsten sulphide (WS_2), boron nitride (BN), molybdenum disulphide (MoS_2), consist of sheets having the thickness in nanometer with extended lateral dimensions. The quantum confinement on the thickness direction exhibits interesting electronic properties and effect of surface chemistry, topography, charge, energy targeted for applications in various field such as switching, catalysis, sensing and energy storage applications [3]. These 2D materials have attracted great attention due to their own space as major categories in the field of nanoscience. Such type of 2D materials were estimated as thermodynamically unstable in the free state, as an evidence of more research have to be done in support of this prediction. Nobel laureate Professor Andre Geim's group was successfully shown the first experimental evidence of observed room temperature quantum hall effect observed at room temperature using a simple method of mechanical exfoliation of Highly Oriented Pyrolytic Graphite (HOPG) in 2005 [4, 5]. Since then, most the researchers all over the world have focused their research on graphene and related atomically thin layered materials. Consequently, the research on graphene become more popular and dominated in field materials science. The first method used by Gim's group to synthesize graphene has few limitations such time consumption and low yield. Therefore, research on graphene was emphasized on large scale production. Different kind of synthesis approaches were used to prepare graphene for examples, metal ion intercalation [6], liquid phase exfoliation of graphite [3, 7], Chemical Vapor Deposition (CVD) growth [8], vacuum graphitization of silicon carbide (SiC) [9], bottom-up organic synthesis of large polycyclic aromatic hydrocarbons (PAHs) [10-12], and chemical reduction of GO [13, 14] and so on. Out of these synthesis approaches, each method has advantages and limitations, however, GO was most suitable material for graphene because of its large scale availability and wet chemical process ability to monolayers.

The fascinating backhistory of GO began before 160 years and it is a synthetic material that cannot occur naturally. British scientist B. C. Brodie identified this material for the first time and named it as graphitic acid or graphite oxide. He developed new chemical route to prepare GO using chemicals such as graphite added with potassium chlorate ($KClO_3$) and fuming nitric acid (HNO_3) [15]. Later on, in the year 2004 when the research on graphene started, GO was also known as graphene oxide Chemically both GO and graphene oxide are almost same since graphite oxide is base material used to prepare graphene oxide. When it come to their structural difference, one can say that a single atomic layer of graphite oxide is nothing but a graphene oxide. It is widely known that GO is dispersed in a specific chemical solvent, as a result it is less partially exfoliated by the solvent molecules, therefore it is called as graphene oxide. In support of this, many experiments were carried out on the synthesis of GO using wet chemical processes, and results obtained from this experiment indicates that large amount of GO flakes in solution was main motive behind these experiments. In other words, GO film or GO powder is called as a graphite oxide in the view point of physics. Henceforth, in the following section, we will use only one common abbreviation for graphene oxide and graphite oxide as GO because chemically they are almost similar as far as their even electronic structures and properties are concerned. But, graphite and graphene are different based on their structural make up.

It is believed that GO is a relatively new kind of materials and considered as non-stoichiometric macromolecule which is chemically hygroscopic and labile in ambient condition depends on the chemical behavior. Interestingly, the several approaches were used to synthesis GO and then modified several times using different chemicals such as concentrated sulfric acid [16], potassium permanganate, even phosphoric acid [17]. It is clearly found that, depending on the protocols used, the chemical composition of resulted compounds having some difference based on the chemical route used during synthesis process.

In general, GO has long last history of 160 years. Even after the inception of new material called as graphene, the details of its chemical structure among research community were not understood well yet. During the last decade, a reasonable amount of research work on GO can be found, which was focused to explain the details of its chemical composition [18, 19]. These research work suggested that GO is a corrugated carbon sheet with over half of the carbon atoms functionalized with epoxy groups and hydroxyl, and edges partially occupied by carboxyl, hydroxyl, ester, ketone and even lactol structures. Despite these, the distribution of functional groups and the spatial connectivity is not addressed yet. These days, the research on Go is becoming more and more popular. Professor Rodney Ruoff in UT Austin invented most popular reagent as a hydrazine for preparation of graphene using chemical reduction of GO [14]. It well understood that bulk GO is an electrical insulator and it transformed into electrically conductive material after the chemical reduction. It is reported that, upon the chemical reduction process of GO in order to prepare graphene, the electrical conductivity has been improved by few orders of magnitude, at the same time, it also exhibit decrement in carrier mobility and poor crystallinity [20] than their mechanically cleaved counterpart [4, 5]. It is equally important to note that the various nomenclatures have been used by the researchers for these materials such as Chemically Modified Graphene (CMG), Chemically Converted Graphene (CCG) or ***reduced Graphene Oxide (rGO)***. For the easiness and simplicity, we will prefer to use the term rGO for these materials in the following discussions. For the preparation of graphene using reduction of GO in chemical oxidation environment leads to the formation

of number of defects as well as vacancies within the sp^2 carbon lattice, which are difficult to almost impossible to improve by means of any further chemical treatments [20, 21]. For this reason, the researchers who were working on GO have focused their research on GO and rGO applications. GO, rGO's and their derivatives shows poor crystallinity upon chemical reduction, but still hold ground for different kinds of emerging applications in the field of energy storage, sensing, water purification, electronics, and so on. From the literature survey on GO and rGO, it is found that few researchers ignore the difference between rGO and high quality graphene, and they claim their results as graphene properties and applications. Therefore, it is worth mention that GO and rGO's has to put into different categories as well as results of rGO must kept as a different topic than research result on graphene.

3.2 Structure of graphene

A hexagonal unit cell of the graphene honeycomb lattice contains two equivalent sub-lattices of carbon atoms bonded together with σ bonds. It has a unique band structure consists of the conduction band and the valence band touch each other at the Dirac point, which shows a ***zero band gap semiconductor*** nature, as shown in Figure 4(a). Each carbon atom in the lattice comprise of a π orbital that contributes to a delocalized network of electrons, whether freely suspended graphene has 'intrinsic' ripples or not has relieved by Monte Carlo simulation [22]. Figure 4 (b) displays the microscopic corrugations were shown by a height displacement of about 0.7 to 1 nm and lateral dimension of about 8 to 10 nm. In addition to the 'intrinsic' corrugations, graphene in real 3D space might have other 'defects', for instance, vacancies, edges/cracks, adsorbed impurities, topological defects (e.g., pentagons, heptagons, or their combination) and so on.

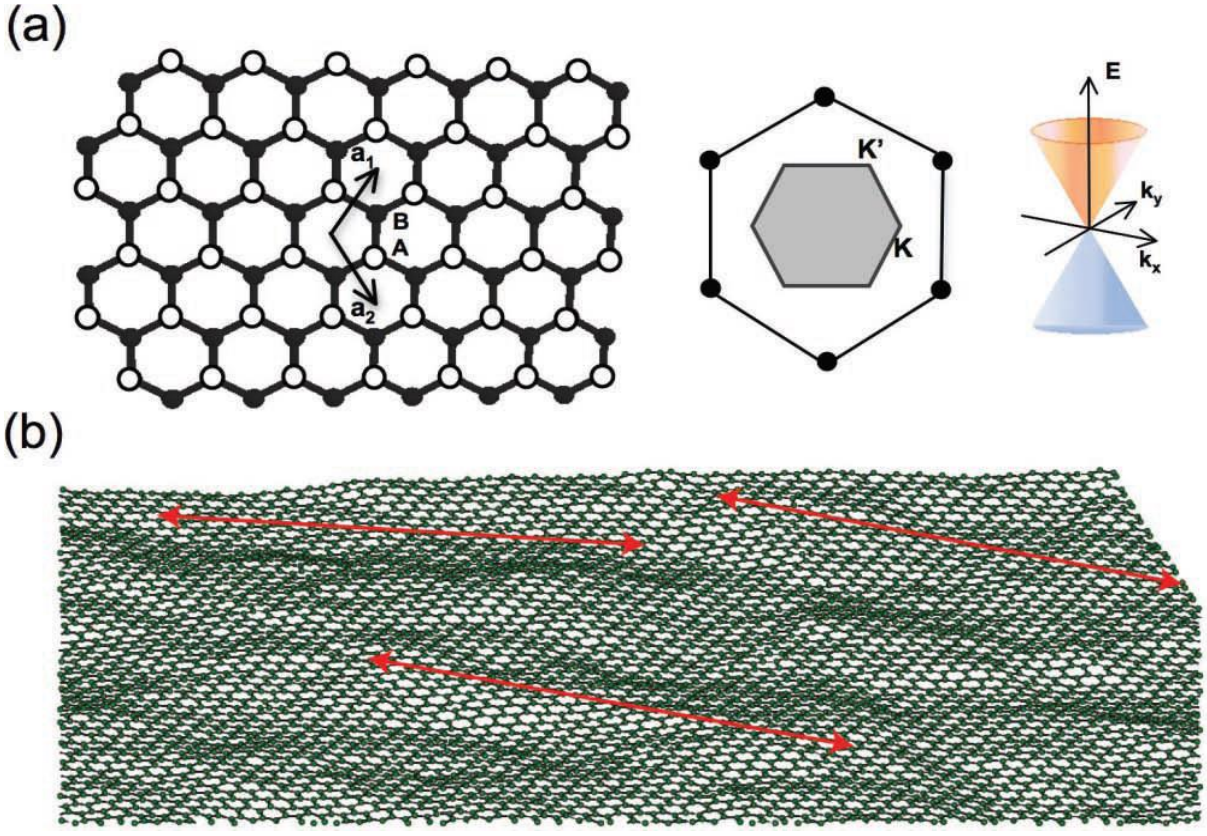

Figure 4. (a) Schematics of the crystal structure, Brillouin zone and dispersion spectrum of graphene; (b) 'Rippled graphene' from a Monte Carlo simulation. The red arrows are ~ 8 nm long. [22]

3.3 Properties of graphene

Table 2. Properties of graphene. [23]

Specific surface area	2630 m^2 g^{-1}
Intrinsic mobility	200,000 cm^2 v^{-1} s^{-1}
Young's modulus	~ 1.0 TPa
Thermal conductivity	~ 5000 Wm^{-1} K^{-1}
Optical transmittance	~ 97.7%

3.4 Structure of graphene oxide (GO)

In recent years, a significant number of review have been published on the preparation of dispersions of graphene oxide platelets and reduced graphene oxide platelets, made from GO. Among these, GO is synthesized by either the Brodie [15], Staudenmaier [25, 26], Hummers method [16] or Tour method [17]. In the following section 3.5 the details of all synthesis procedures are explained. Figure 5 is schematic of a proposed structure of graphene oxide that is supported by solid-state nuclear magnetic resonance (SSNMR) experiments on 13 C-labeled GO and various models proposed for the structure of graphene oxide [24].

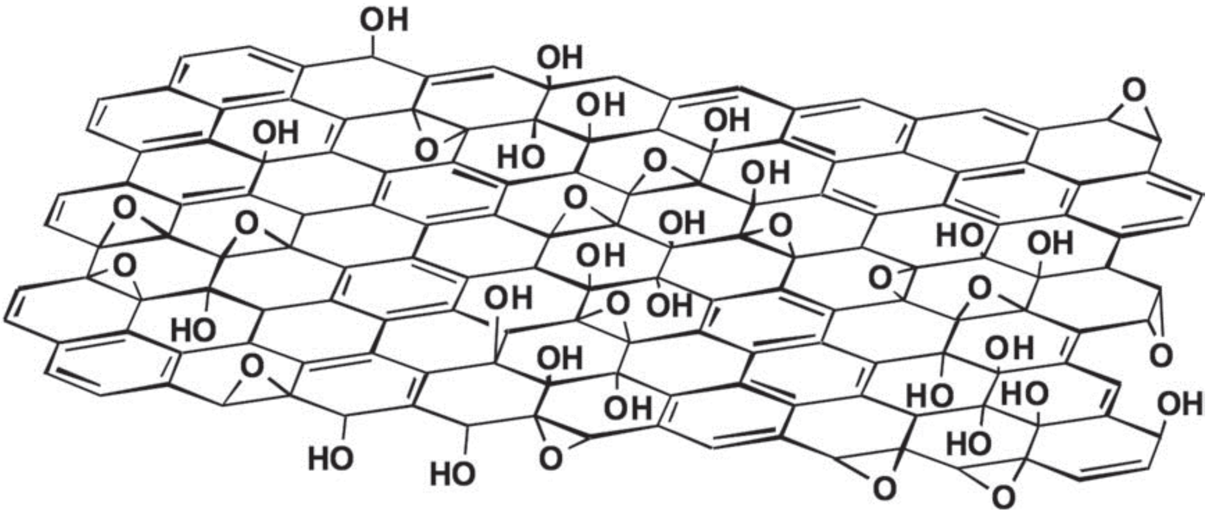

Figure 5. A proposed schematic (Lerf-Klinowski model) of graphene oxide structure. [24]

3.5 Synthesis methods of GO & rGO

This section deals with the four different types of approaches used for the GO preparation in the chronological order, and discuss and compare their chemical processes in detail. These synthesis methods include 3.5.1 Brodie Method and Staudenmaier Method, 3.5.2 Hummers Method and Its Modification, 3.5.3 Tour Method and Discussions.

3.5.1 Brodie method and Staudenmaier method

In 1859, a British researcher B.C. Brodie who invested the chemical method to prepare GO for first time while he was investigating the chemistry of graphite [15]. He prepared the mixture of $KClO_3$ and slurry of graphite into fuming HNO_3, then he obtained a new type of compound which consists of oxygen, hydrogen and carbon. Then resultant compound was washed in order to avoid any impurity such as salts produced in the chemical reaction. After

that, it was dried at 100 °C, and consequently put it under oxidation environment. It was observed that new type of compound undergoes an appearance change in the following three repeated treatments. Additionally, resulted in a substance with a "light yellow color" which would not change with any additional oxidation treatment. He realized that the new compound could not be prepared again by one prolonged treatment, but it required the oxidation process with the restoration of the original conditions each time.

Elemental analysis of new compound suggested that the molecular formula was $C_{11}H_4O_5$. Moreover, mild dispersability and weak acidity in basic solution was observed as well as the reflective goniometry characterization failed due to the limited thickness, imperfect structure and small size. In addition, the final product was reacted with "protochloride of copper and protochloride of tin" to obtained GO salts, and then summarize with the analysis in composition and then thermal decomposition in detail. His observations and conclusions were limited by the theories and characterization techniques available during that period, which opens the door of huge room for us work and improve today.

First attempt to make some modification to improve the Brodie's method was made by L. Staudenmaier in 1898 [25, 26]. Two main modification was suggested by L. Staudenmaier: 1) addition of multiple aliquots of potassium chlorate solution into the reaction mixture during the chemical reaction; 2) addition of concentrated sulphuric acid to increase the acidity of the mixture. Such kind of modification result into a highly oxidized GO product in a single reaction vessel. This make simplified GO synthesis process on large scale.

Nevertheless, Staudenmaier's method had two major limitations; one is hazardous and another is time consuming. It is found that the addition of potassium chlorate required a more time over a week and the by-product gas (chlorine dioxide) evolved during the reaction required to be removed by an inert gas, whereas explosion was a constant hazard. Thus, any further changes, development or modification to improve this oxidation process was still under investigation.

3.5.2 Hummers method and its modifications

Another attempt to method to prepare GO was investigated by Chemists Hummers and Offeman in Mellon Institution of Industrial Research developed with a modification in synthesis process has been made in 1958 [16]. This method suggests that a water-free mixture of sodium nitrate, concentrated sulphuric acid and potassium permanganate was prepared and maintained below 45°C for graphite oxidation. The duration of whole oxidation process was about two hours, and result to a final product with higher degree of oxidation than GO prepared by Staudenmaier's method as shown in Table 3.

Table 3. Comparison of Staudenmaier GO and Hummers GO in chemical compositions. [16]

Method	Carbon (wt %)	Oxygen (wt %)	Water (wt %)	Ash (wt %)	C/O atomic ratio
Acid-permanganate-nitrate	47.06	27.92	22.99	1.98	2.25
Staudenmaier	52.11	23.99	22.22	1.90	2.89

But, in case of Hummer's method, end product contain incompletely oxidized graphite core with GO shells as well as a pre-expansion process play an important role to obtain higher degree of oxidation. In 1999, for the first time Kovtyukhova reported a pre-treatment of graphite using a solution of concentrated H_2SO_4, $K_2S_2O_8$, and P_2O_5 at 80 °C for several hours which was widely accepted by researchers. According to this pre-treatment a solution was diluted, filtered, washed and dried prior to the Hummers oxidation step. One more prominent change in the preparation of GO suggested to use high amount of the potassium permanganate [13]. Currently, this modified Hummers method which is a chemical process is widely accepted technique among the researcher all over the world to prepare GO as shown in the figure 6. In general, end product of GO prepared using this modified method includes thin flakes of GO having the thickness of about 1 nm which resembles to a single layer, and lateral dimension about 1 micron in average and the chemical composition was found to be to be C:O:H = 4:2.95:2.5 [27]. Thus, the oxidation degree and yield of GO have been significantly increased improved as compared to first ever method discovered by Brodie. In contrast, the modified Hummers method consist of the separation and purification processes which are still considered as relatively complex and time consuming.

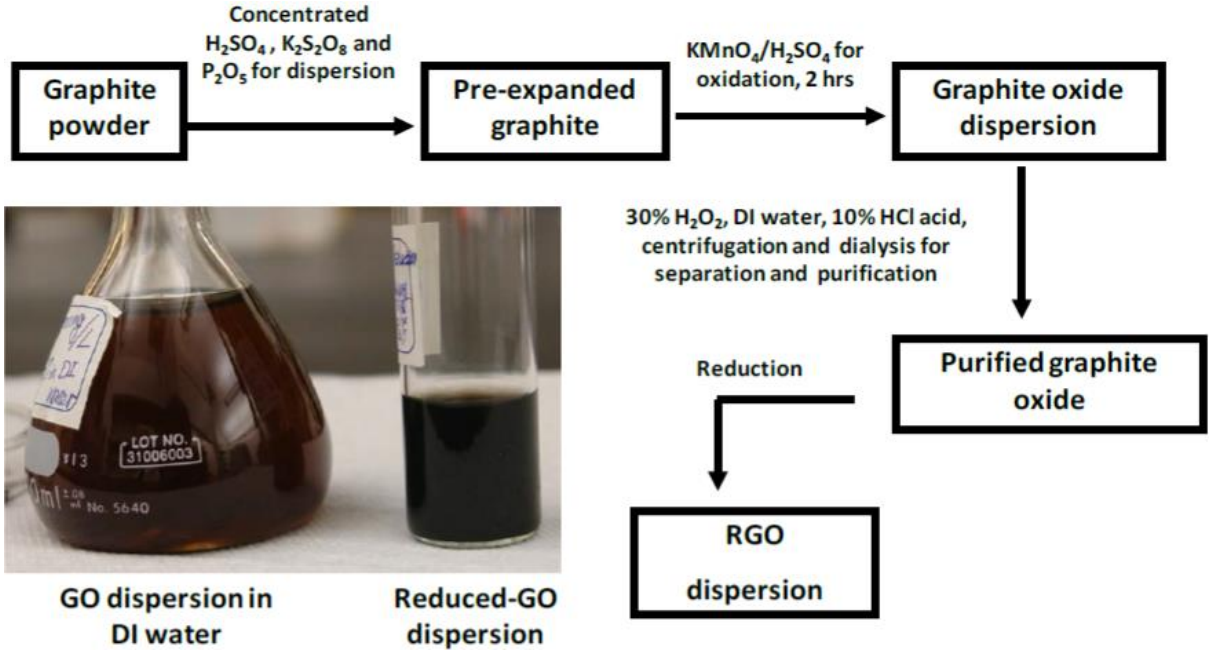

Figure 6. A Schematic of modified Hummers method for GO preparation. [16]
Lower left: photographic images of the final product GO in deionized (DI) water (left) and the dispersion after hydrazine reduction with ammonia (right)

3.5.3 Tour method

The research era of graphene began in 2004, since then research on GO become more popular research topic in the field of carbon related materials. Significant numbers of the research reports published were emphasized on its structure, reduction and applications. As part of further development, a new method was proposed by American Professor of Tour's group in Rice University in 2010. In this method, sodium nitrate was replaced by new material called as phosphoric acid while high amount of potassium permanganate used during the chemical reaction process [17]. They have claimed that end GO product is obtained with higher degree of oxidation using a chemical reaction of graphite and six equivalents of $KMnO_4$ with a mixture having the ratio 1:9 of H_3PO_4/H_2SO_4. The biggest advantages of this method is the replacement of $NaNO_3$. Since $NaNO_3$ was not participated in the chemical reaction, the hazardous and toxic gases such as N_2O_4, NO_2 or ClO_2 were not created. Therefore, this method became eco-friendly. In addition to this, phosphoric acid provides a platform to intact graphitic basal planes and as a result the end product with higher yield is received as compared to that of Hummers method. Figure 7 shows the comparison between these methods according to the ref [17].

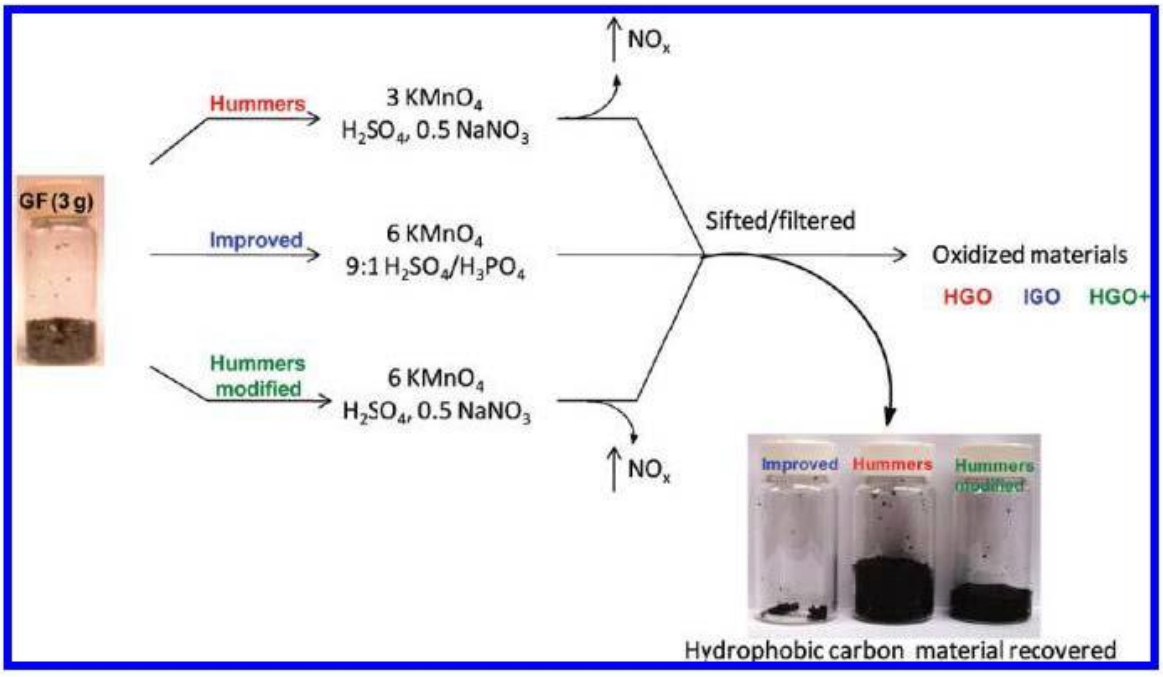

Figure 7. A comparison of procedures and yields among different GO preparation recipes. [17]

3.5.4 Oxidation mechanism

Graphite source is main component during the chemical process used for the synthesis of GO. The most common source to extract of graphite come from naturally occurring mineral which has been purified to remove heteroatomic impurities such as iron and sulphur. Despite this, specific defects found in the crystalline structure which could be acts as initial sites for

chemical oxidation. However, it is difficult to explain the exact oxidation mechanism in occurred in chemical reactions because of the natural defects and complexity of the structure. Also, graphite nanofibers were widely applied as a starting material to prepare GO which results into the formation of uniform GO nanosheets in size distribution. It is believed that the coin-stacked graphene planes along the length of the fibers plays a vital role, and tunability of the GO size upon oxidation time was reported [28].

Till today, two different type of approaches of oxidation reagents were applied in order to oxidize graphite into GO, one was nitric acid with potassium chlorate while another was sulphuric acid with potassium permanganate. From the literature survey, it is clear that the nitric acid could react with aromatic carbon surfaces such as carbon nanotubes [29] and fullerenes [30], which were responsible for the formation of different oxygen containing functional groups such as lactones, carboxyl's, ketones whereas toxic gases such as NO_2 and N_2O_4 were released. In the same way, potassium chlorate offers its oxidation capability during chemical reaction by producing reactive species of dioxygen [31]. The chemicals incorporated for the fabrication of GO using Brodie method and Staudenmaier method were supposed to be the strongest oxidizers. Further, for the second combination of $KMnO_4$ and H_2SO_4, permanganate ion can also serve as oxidation reagent. The MnO_4^- can become more reactive in acidic solution as shown in in the following chemical reaction [32]:

$$KMnO_4 + 3H_2SO_4 \rightarrow K^+ + MnO_3^+ + H_3O^+ + 3HSO_4^-$$

$$MnO_3^+ + MnO_4^- \rightarrow Mn_2O_7$$

Scheme 2. Formation of dimanganeseheptoxide from $KMnO_4$ in the presence of strong acid. [32]

The formation of reactive Mn_2O_7 from MnO_4^- actively participate to support to oxidize graphite, however the bimetallic form of manganese oxide could be exploring when temperature reached to 55 °C or it came in contact with organic compounds [32,33].

The latest acid that used for the preparation of GO was phosphoric acid, which is supposed to have an advantage to help 6-membered rings unchanged in the basal planes of the final product [34]. While the formation of the 5-membered phosphor ring offers support to control further oxidation of the diols. This advantage could be well explained as shown in figure 8 and as reported in Ref. [34].

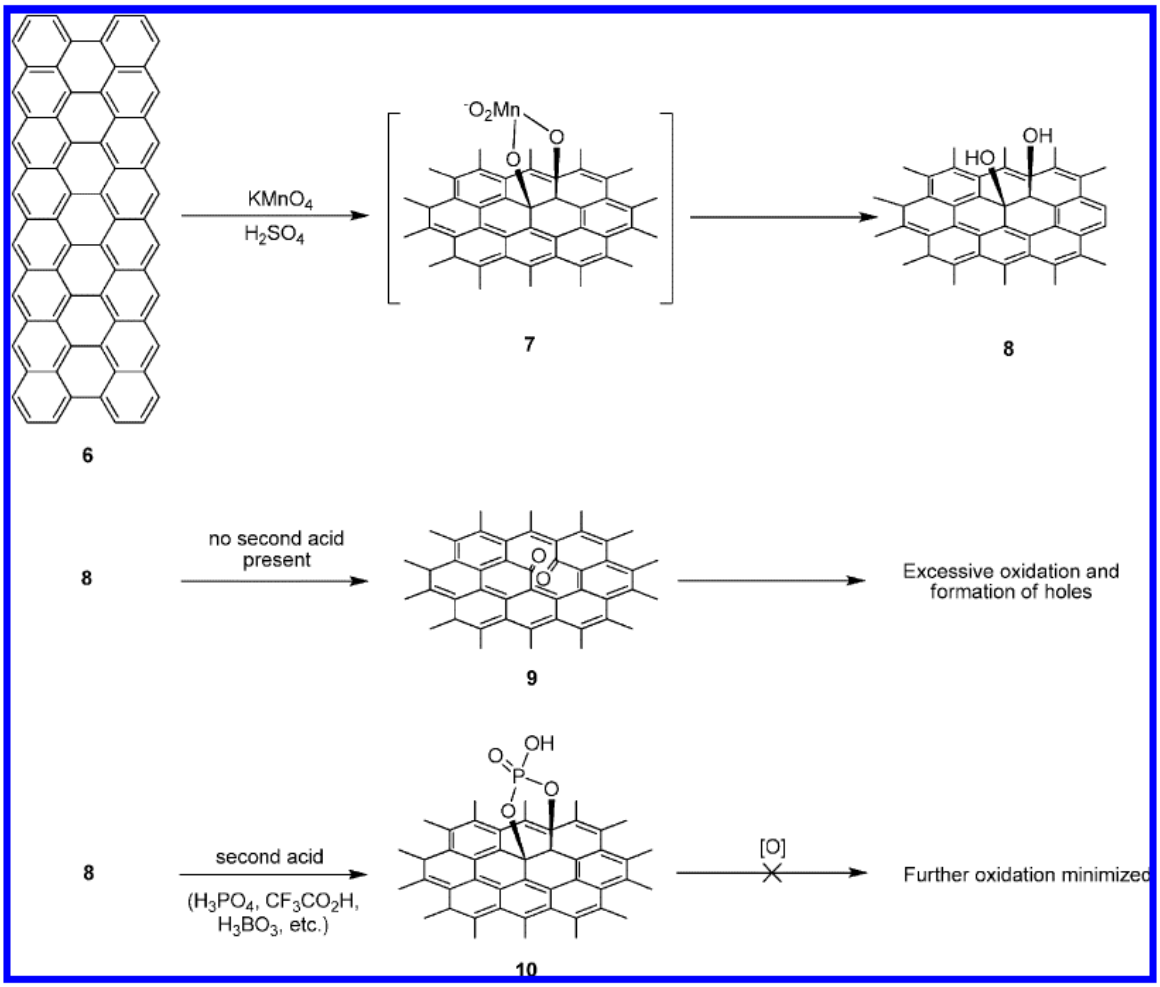

Figure 8. Proposed mechanisms for the effect of the second acid in prevention of over-oxidation of the sp^2 carbon network once they have formed the vicinal diols. [34]

During the fabrication of GO, purification is equally important but monotonous step because it needs various process like washing, filtration, centrifugation and dialysis. According to the published reports, it is showed that the GO could contaminate with potassium salts which is highly flammable could causes a fire hazard. It is believed that the volume expansion and gelation occurred while washing of GO using water greatly slows down the purification process, and a substitution with HCl acid and acetone as suggested by Kim et al. [35].

To sum up, in the section devoted to the history of GO synthesis includes four different approaches recipes have been introduced while remaining part describes the improvements in simplicity, yield, oxidation and the product qualities. These days, preparation of GO is not a difficult task, it certainly helps in making advances in GO research. But, some issue such as basic understanding of the oxidation processes and detailed mechanisms have not fully addressed yet. This could be major difficulty which is stopping us from improving synthesis conditions using various possible chemical reactions and manipulating the reaction to deal with some technology issues, such as size distribution control, edge structure selectivity, band gap tuning etc.

4. Introduction of photocatalysis

Photocatalysis word arises from two different words: light and catalysis. Among the all the possible various definitions available today, most commonly used definition is: chemical reaction induced by photo-absorption by a solid material (mostly a semiconductor). At the surface of the semiconductor, the reaction occurs could not show any changed during and after the reaction. Here, the reactant semiconductor material is called a 'photocatalyst'. It is well known that the catalysis and the photocatalysis are two different physico-chemical phenomena, from a thermodynamically point of view. The function of 'catalyst' is to increase the reaction rate of an already thermodynamically allowed chemical reaction by reducing the activation energy. At the same time, credit must go to energy created by light, photocatalysis can promote thermodynamically unfavorable chemical reaction. The most common example is photocatalytic splitting of water into hydrogen and oxygen [36,37].

Nowadays, organic pollutants present in industrial waste water are a major environmental risk. The release of hazardous minerals from these wastes into the environment causes the contamination of both soil and ground water. These pollutants have threat due to their stability, solubility, toxicity, bioaccumulation capacity and carcinogenic nature which could create serious problem for human health and water related ecosystems. These reasons indicate us towards the urgent need to remove such kind of pollutants by developing some approaches and it became a serious topic of powerful research [38].

Graphene is an interesting and unique material and it is strong candidate as a photocatalytic material because of its zero-bandgap semiconducting property and high electrical conductivity where both electrons and hole are considered as charge carriers with high mobility. Hence, outstanding properties exhibited by graphene such as high electron mobility, high adsorption capacity, make a material of choice for photocatalysis in the degradation of environmental pollutants. Whereas, reduced graphene oxide (rGO) has the ability to transfer and store electrons by a step-wise transfer process and increases its properties. In addition to this, it also serves as a good platform to support the synthesis of semiconductor/metal nanoparticles for photocatalytic degradation of wastes from liquid medium. At this moments, most of the research work have focussed on the use of semiconductor with noble metal nanocomposites for the photocatalytic degradation of water pollutants [39].

5. Characterization methods

5.1 Ultraviolet-visible spectroscopy (UV-Vis)

For any physical substance, color is an important feature. For example, polytetrafluoroethylene is white, graphitic materials like graphite, graphene, carbon nanotubes are grey. Metals possess various colors depending on different structures. To analyse the light reflection from solid surface or passing through a liquid, human eyes act as spectrometers for differentiating the matter by color. In the ultraviolet, visible and infrared regions of the electromagnetic spectrum, sunlight or white light is actually composed of a broad range of radiations. When white light is passed through a colored substance, the amount of light is absorbed by substance and the color of the substance recognize by human eyes is determine by the remaining light which is complimentary to the absorbed light. For example, if a substance absorbs indigo light from 420 to 430 nm, it appears yellow; while the substance absorbs green light from 500 to 520 nm, it appears red in color [40].

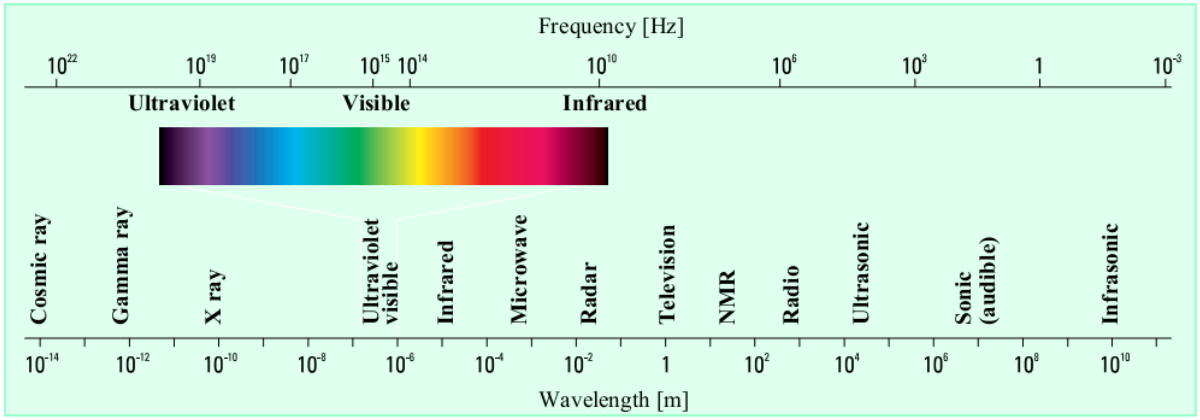

Figure 9. The electromagnetic spectrum. [41]

The electromagnetic spectrum (Figure 9) is very broad ranging from cosmic ray (short wavelength) to infrared sonic ray (long wavelength). The ultraviolet radiations (10 nm-400 nm) and visible radiations (400 nm-800 nm) represent only a small portion in the spectrum. However, less than 200 nm ultraviolet radiations are difficult to handle. UV-Vis light energies ranging from 1.55 eV to 6.20 eV corresponding to wavelengths of 800 nm and 200 nm, respectively. Such energies are enough to cause electronic transitions in molecules, from low energy orbitals to high energy orbitals. The electronic transition occurs, when the energy of light matches the gap between two energy levels and light gets absorbed.

Under UV-Vis irradiation, $\pi \rightarrow \pi^*$ transition in –C=C- bond and $n \rightarrow \pi^*$ transition in C=O bond occurs. Since, graphene oxide contains many such bonds, Ultraviolet-visible (UV-vis) absorption spectroscopy is a useful technique to monitoring the structural changes during synthesis of GO and further reduction.

5.2 Scanning electron microscopy (SEM)

Scanning electron microscopy is a type of electron microscopy in which, image of sample is produced by scanning it with a focused beam of electron. The topography and composition of the surface of sample are attained by collecting various signals produced by interactions between the atoms of sample and electron beam. M. Ardenne invented the first scanning electron microscope in 1937, and first commercial SEM instrument was developed by Cambridge Scientific Instrument Company in 1965.

Detecting secondary electrons emitted from the k-shell of the specimen atoms by inelastic scattering interactions with beam electrons, is the most common and important imaging mode of SEM. Other imaging modes include transmitted electrons, backscattered electrons, specimen current, electron-beam-induced current, acoustic thermal-wave microscopy, cathodoluminescence, imaging with X-rays and environmental electron microscopy. Conductive and non-conductive, both samples can be imaged by SEM [42].

5.3 Raman spectroscopy

Raman scattering and infrared absorption are the main spectroscopies which deals with molecular vibrations. These spectroscopies are widely used to give the information of chemical structures of substances by their characteristic spectral analysis. The elastic scattering

phenomenon was firstly observed experimentally by Raman and Krishnan in 1928. Raman spectroscopy has been developed further from this phenomenon.

In infrared spectroscopy, an infrared beam between 400~4000 cm^{-1} frequencies are directed on the sample; when the frequency of incident radiation matched to a molecular vibration, an absorption occurs. On the other hand, in Raman spectroscopy, a single frequency of radiation (514 nm or 633 nm or 785 nm) is employed and the radiation scattered from molecule is detected. Intense infrared absorption occurs when vibrations cause changes in the dipole moment of the molecule, while intense Raman scattering occurs when vibration cause changes in the polarizability of the electron cloud around the molecule. Therefore, infrared and Raman spectroscopy are complementary and generally used together to give a better characterization of the molecular structure [43].

5.4 X-ray diffraction spectroscopy (XRD)

X-rays are electromagnetic radiation in the range of 100 eV - 100 keV with typical photon energies. Only short wavelength x-rays (hard x-rays) in the range of a few angstroms to 0.1 angstrom (1 keV - 120 keV) are used for diffraction applications. They are ideally suited for probing the structural arrangement of atoms and molecules in a wide range of materials, because the wavelength of x-rays is comparable to the size of atoms. The energetic x-rays can provide information about the bulk structure by penetrating deep into the materials.

X-rays are produced generally by either synchrotron radiation or x-ray tubes. In an x-ray tube, x-rays are generated when a focused electron beam accelerated across a high voltage field bombards a rotating or stationary solid target. A continuous spectrum of x-rays is emitted, as electrons collide with atoms in the target and slow down, which are termed Bremsstrahlung radiation. Through the ionization process, the high energy electrons also eject inner shell electrons in atoms. An x-ray photon with energy characteristic of the target material is emitted, when a free electron fills the shell. Common targets used in x-ray tubes include Mo and Cu, which emit 8 keV and 14 keV x-rays with corresponding wavelengths of 1.54 Å and 0.8 Å, respectively [44].

5.5 Femtosecond transient absorption spectroscopy (fs-TAS)

5.5.1 Introduction

A lot of research is directed in physics, chemistry and biology, to understand the dynamics of various processes. System parameters change over the time. Time scales on which the parameters are changes, may vary from very slow to the extreme faster, depending on the size of the object being watched. Figure 10 shows different natural processes, their timescales and instruments changing over the time.

In order to follow the different processes, different tools are required. Calendar is probably a slowest tool. Film cameras or photographic cameras with short exposure time, are used to record the faster events. Electronic devices provide the time scale access from microseconds, nanoseconds, up to the hundreds of picoseconds. In faster processes, the fastest tool available in nature is ‘light’ itself. Speed of light in vacuum is roughly 3×10^8 m/s. The processes happening faster than 1 μs are considered as an ultrafast processes. Ultrafast processes explored by the area of science in molecules, atoms, glasses and crystals using light based spectral techniques is called ultrafast spectroscopy (also called as time resolved spectroscopy).

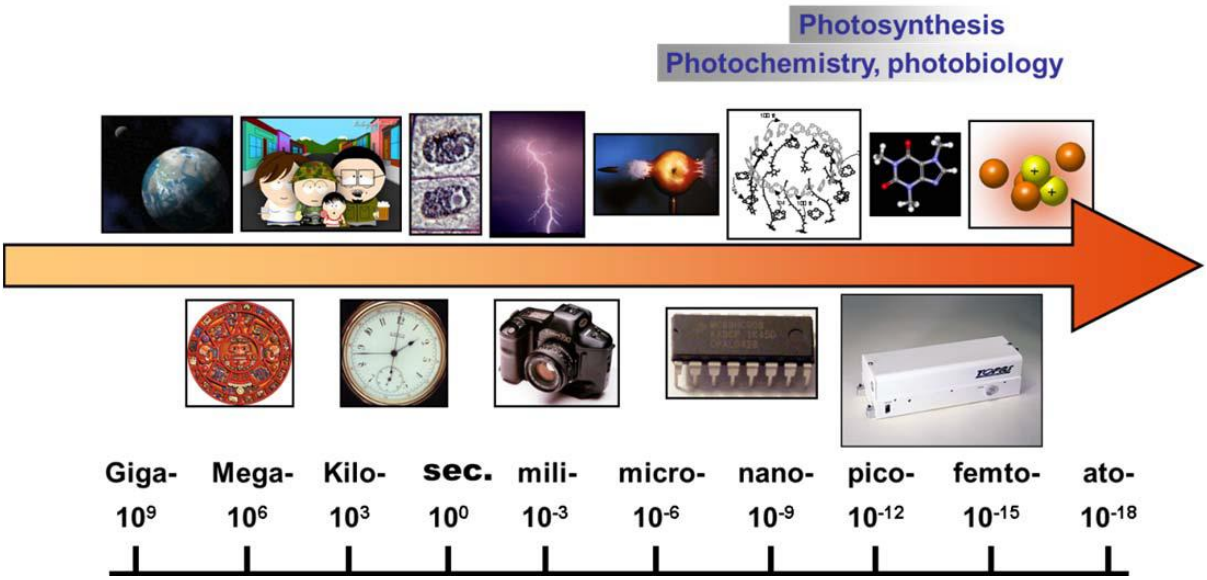

Figure 10. Different natural processes, their timescales and instruments for following them. [45]

5.5.2 Principle

Among spectroscopic methods, transient absorption spectroscopy (TAS) is one of methods for observing the time change of various photochemical reactions caused by light-excited molecules and solids. The principle of this method is to detect absorption contributed from a short-lived reaction intermediate generated by excitation light by using probe light. It is possible to trace the formation / disappearance of various short-lived reaction intermediates by selecting as the probe wavelength which specimen you want to observe absorbs. In the measurement at the time scale of femto to nanoseconds, time resolved measurement is made possible by using short pulsed light for both pump light and probe light.

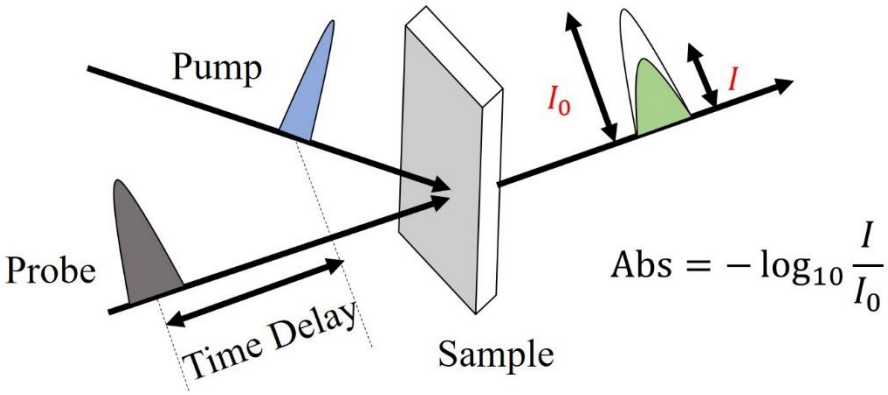

Figure 11. Principle of Femtosecond transient absorption spectroscopy.

Figure 11 is the principle of femtosecond transient absorption spectroscopy. The sample is excited with the pump light, and the intensity of the incident probe light is detected with delay time. Also, the intensity of the probe light is measured when specimen is not excited, and the transient absorption intensity is obtained by the Lambert-Beer law.

5.5.3 Light source for ultrafast spectroscopy

For obtaining powerful laser pulses, technique is used called Q-switch or a variable attenuator in the laser cavity. Basic idea of the technique is introducing variable losses in the laser cavity. The name Q-switch derived as, changes in losses calculated in the different quality factor of the laser cavity. For light, pumped active medium acts as an amplifier, positive feedback provided by the cavity mirrors, returning part of the produced light into the active medium. The light, that has left the active medium cannot come back and the positive feedback required for lasing does not occur, when cavity losses are on. Because of that, hard pumping of active medium does not result in lasing. The Q-factor of the cavity suddenly increases when the losses are switched off and the laser starts lasing. The gain of the amplifier is very high and the intensity of laser radiation grows extremely fast, because the active medium has stored a large amount of energy. High intensity radiation produced quickly all the population inversion, because it disappears very fast. In this way, giant pulses are produced. Generally, Q-switched lasers as Nd:YAG or Nd:YLF produced by different companies as their active media; the pulses produce with the duration around 10 ns, with the excess of 1 J energies.

Q-switching is generally performed by using one of the three crucial methods. The variable loss components of the cavity depend on:

- Saturable absorber
- Acousto-optic modulator
- Electro-optic modulator

An electro-optic Pockels cell is one of the most common active Q-switches. The high voltage is inducing birefringence and act as a half-lambda phase plate. In another words, the phase difference between an ordinary and extraordinary waves becomes equal to π, passing the crystal. Polarization plane gets rotated by 90°, when linearly polarized light impinges on such crystal at with its polarization axis at 45° to the ordinary axis. A polarizer is inserted into the cavity, along with a crystal. The polarization of light generated in the cavity is such that the polarizer blocks it, when the high voltage is off; the losses of the cavity are high and no lasing can occur. The light polarization is rotated and the beam can pass through the polarizer without losses, when the gain medium accumulates enough population inversion, half-lambda voltage is switched on. It results in a giant light pulse, which sweeps down the accumulated population inversion. Pockels cells, shown in figure 12 (B), are called active because they are actively controlled by an external high voltage source. It is used in lasers with different repetition rates from several Hz to 1 MHz.

Acousto-optic modulator is another type of an active Q-switch. It consists of a piece of transparent material like glass or quartz, by using piezoelectric effect a standing acoustic (ultrasound) wave is produced. Transparent material is attached to a piezoelectric transducer. Periodic modulation of refractive index in the material is produced by standing acoustic wave by a phase grating. By this grating laser radiation is diffracted and it changes direction of propagation and leaves the cavity. All the light is transmitted by the transparent material when RF field is switched off and the grating disappears. Giant laser pulse shown in figure 12 (C), is produced when the lasing starts. Pulses of hundreds of nanoseconds produced by acousto-optic Q-switches.

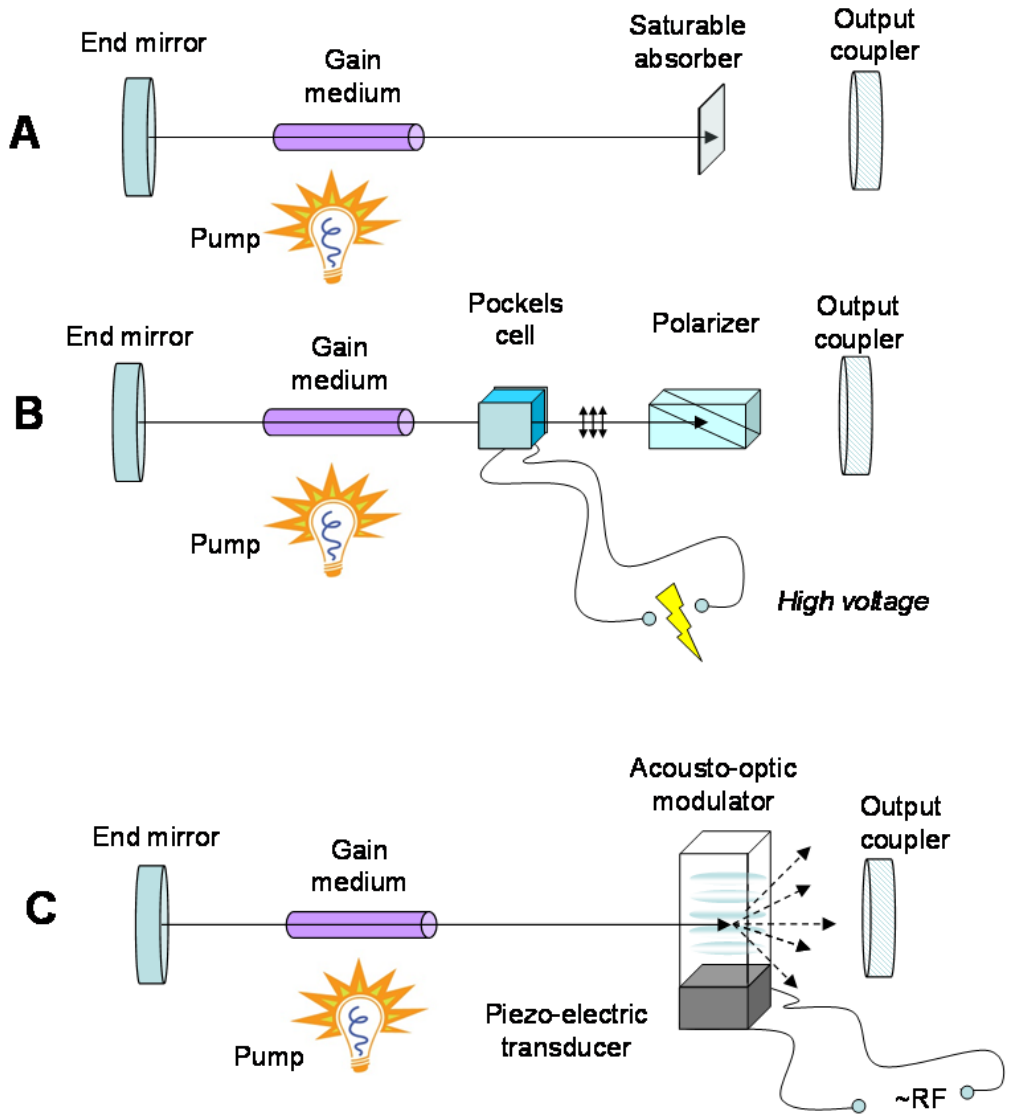

Figure 12. Laser cavities with different Q-switches. (A) saturable absorber, (B) Electro-optic modulator (Pockels cell), (C) Acousto-optic modulator. RF denotes radio frequency electrical field used to excite piezoelectric transducer and generate a standing acoustic wave in the crystal. [45]

Simplest and most widely used mode-locking mechanism in Ti:Sapphire laser systems is Kerr lens mode-locking. Kerr effect is the dependence of refractive index of a medium on the light propagating intensity. Similar to Gaussian (i.e. the intensity is low at the sides and high at the center), a laser beam intensity distribution in the plane perpendicular to the beam propagation direction. The refractive index change is highest in the center and lowers at the edges, when such beam propagates in the medium with nonlinear refractive index. The beam starts to focus, when the medium obtains refractive index profile similar to that of a lens, as shown in figure 13 (A). The stronger lensing effect can be achieved, when the focusing is tighter, and the intensity of the beam is higher. Accordingly, when the beam starts to self-focus, it will keep contracting in size until diffraction or breakdown of the medium will kick in to limit the focus. As the refractive index change is proportional to the intensity, the self-focusing is only possible at high light intensities. Now, the intensity will always be higher in the pulsed regime, as the amount of pump light is same; where all the energy is concentrated at the highest

pulse, rather than spread over time. This means that, when the laser is mode-locked, self-focusing will be a lot stronger; because all modes are in phase and strong pulse is generated instead of continuous wave operation.

Figure 13 (B) shows mode-locking in the laser cavity using Kerr lens. The peak intensity in the pulse is higher, when laser operates in pulsed mode (modes are in phase). Kerr lens focuses the beam allowing it to pass the spatial filter and lasing is efficient (thick black line represent the beam). In continuous wave mode, electric field intensity is insufficient for self-focusing to occur and lasing does not start because of the losses on the spatial filter (thin dashed line).

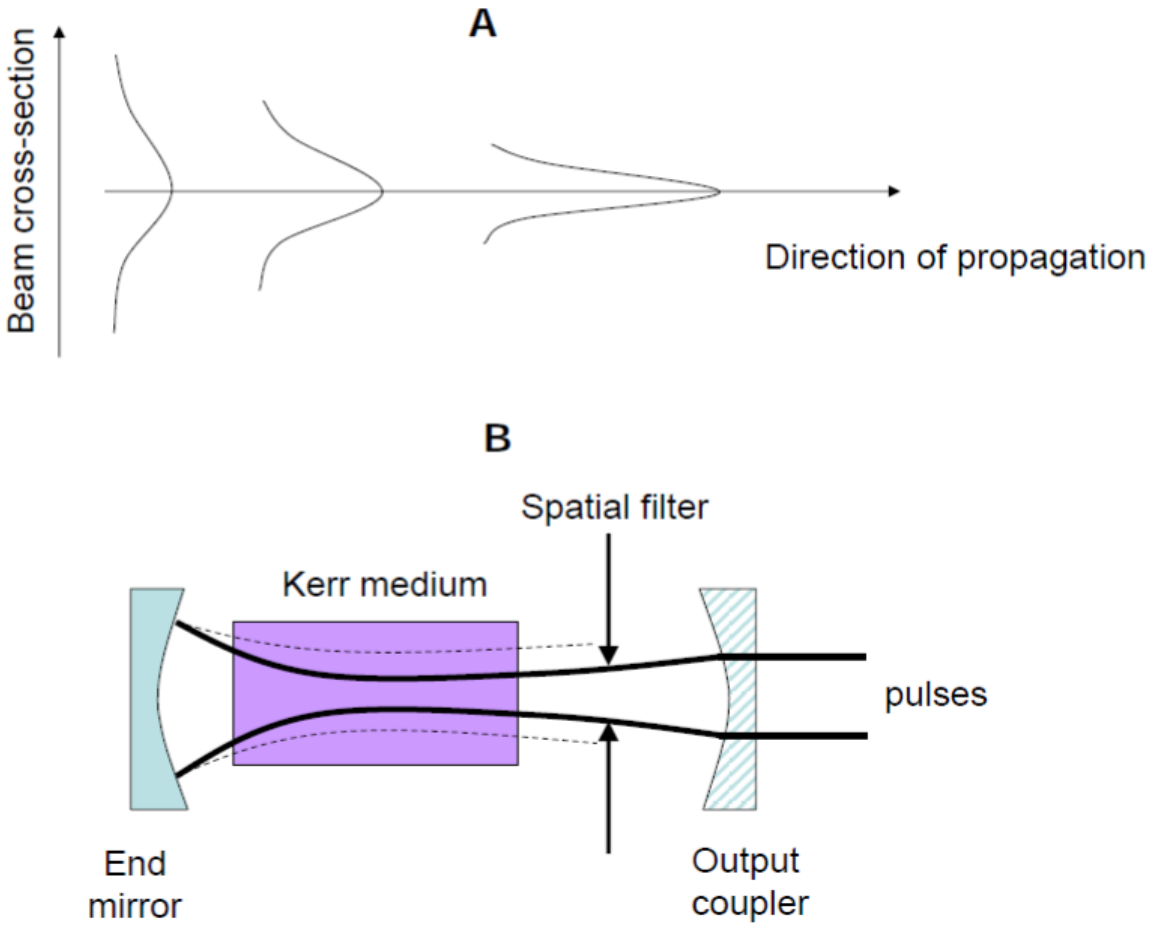

Figure 13. (A) focusing of light due to Kerr effect, (B) mode-locking in the laser cavity using Kerr lens. [45]

5.5.4 Transient absorption spectrum

Transient absorption signals contain several different contributions. For that, the energy level scheme of a hypothetical molecule shown in figure 14 (A). When the sample is excited by the pump pulse, some molecules are transferred to the excited state, shown by solid green arrow in figure 14 (A). This means that part of ground state absorption signal disappears and the concentration of ground-state molecules decreases. Therefore, the absorption difference becomes negative at the wavelengths of ground state absorption. The spectral shape of this

negative contribution measured by a spectrophotometer, which is identical to the ground state absorption spectrum. The difference absorption signal of this contribution is called *ground state bleaching* (GSB). It is shown in figure 14 (B) by green area curve. Until all the excited molecules return to the original ground state from which they were excited this signal remains present.

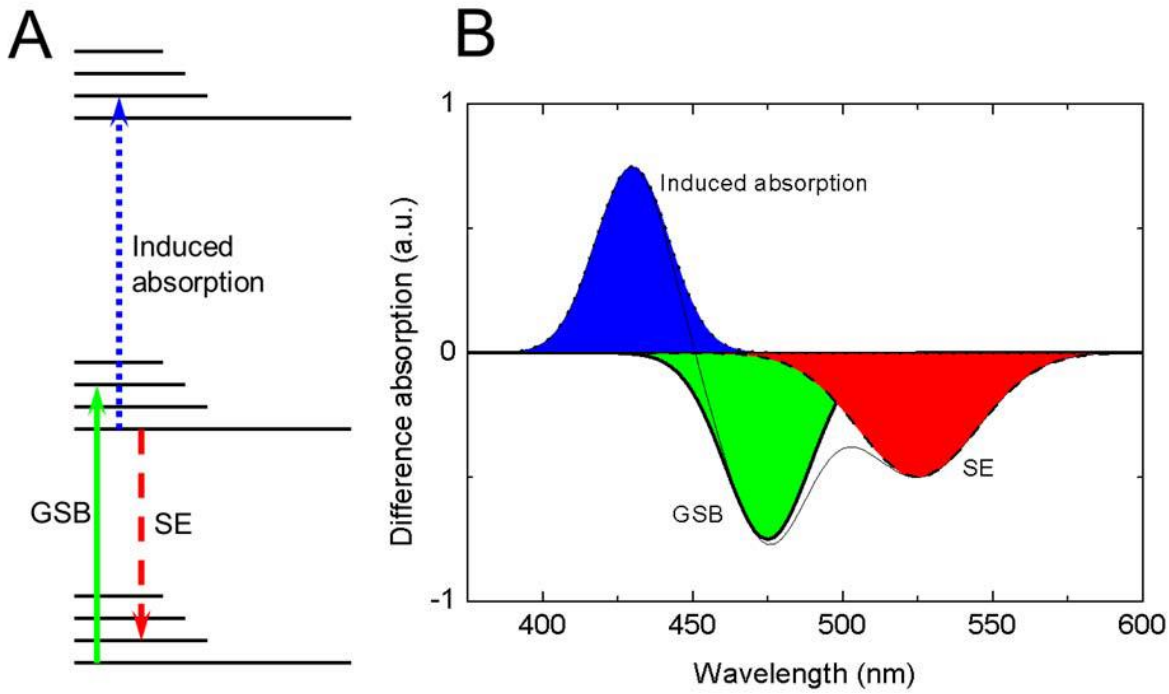

Figure 14. (A) Energy levels of a hypothetical molecule and some quantum transitions influencing the difference absorption spectrum. (B) The corresponding difference absorption spectrum and with separated contributions of different transitions. [45]

Another contribution to the transient absorption signal is related with *stimulated emission* (SE). When the probe pulse finds some of the molecules in the excited state, this signals arises and the photons of the probe pulse stimulate the emission of the sample molecules. Shown by red dashed arrow in figure 14 (A). As the photons that dropped the molecules from the excited to the ground state, radiated by the molecules have exactly the same direction, wavelength and polarization. The detector will receive all these photons plus the photons emitted by the sample, when the laser is mode-locked. The sample emits light and that is found as decreased absorption.

The third contribution to the transient absorption signal is *induced absorption* (IA). It shows the fact that the molecules in the excited state can absorb another photon and go to a higher excited state, shown by dotted blue line in figure 14 (A). After the excitation, additional absorption appears and the related contribution to absorption signal is always positive, because this process can only occur in the excited molecules. Absorption is shown by blue area curve in figure 14 (B). It is noted that, induced absorption is not only caused by singlet excited states of molecules, but the excited molecules have undergone the intersystem crossing to the excited states and triplet state absorption will be observed. This is the advantage of transient absorption spectroscopy, that even if the molecule is back in the ground state, but this state is slightly different from the initial one and we will observe induced absorption of the new ground state.

5.5.5 The dynamics of transient absorption spectrum

The interpretation of kinetic and spectral information of difference absorption spectra is quite simple. A difference absorption spectrum will appear after the excitation of the molecule, and uniformly decay with a characteristic time, equal to the lifetime of the excited state. However, in real life, the molecules are more complex than this: they jiggle around, interact with their environment like solid state matrix, protein, solvent, etc. All types of processes may appear after the excitation and they all influence the difference absorption spectrum one or another way.

Following are some processes:

5.5.5.1 Internal conversion and vibrational relaxation

The molecules consist a different number of electronic states, each of which consist its vibrational sublevels. At higher vibrational sublevels of an electronic state, the molecule is excited, it seeks to establish the Boltzman distribution and the molecule will relax to the lower vibrational sublevels. The transient absorption spectrum will reflect this relaxation, since the energy of the excited states is decreasing during such relaxation. For example, at each time instance, the wavelength of SE depends on the energy gap between the ground state and the excited state occupied at that particular instance. In the induced absorption signal, vibrational relaxation can also be observed, because the wavelength of the induced absorption matches the energy gap between the higher excited state and the excited state occupied at that particular instance. Therefore, we will observe the induced absorption corresponding to transitions S_2 to S_{3+n}, when we put the molecule, say in S_2 electronic state; and this induced absorption signal will disappear and the absorption corresponding to S_1 to S_{1+n} transitions will appear, when the molecule relaxes to S_1.

Additionally, stimulated emission and induced absorption spectra become broader, if the ensemble of molecules (in macroscopic samples we always work with an ensemble) is distributed in a number of different vibrational states. All the molecules of the ensemble gather in their lowest vibrational states, and the broadening decreases, when vibrational relaxation takes place. Even if the particular realization depends on the molecule, it is safe to say that stimulated emission and induced absorption spectra are sensitive to the energy redistribution among the vibrational degrees of freedom in the molecule.

5.5.5.2 Solvation and the relaxation of the environment

Corresponding to the spatial configuration of its nuclei and electrons, each molecule has a certain charge distribution in the ground state. Molecular configuration adjusts the charges of the environment (for example, solvent, protein, etc.) in such a way that the overall energy of the system is at its minimum. The configuration of its electrons is instantly changed, hence the charge distribution occurs after the excitation of the molecule. After that, the environment charges readjust first their electrons, and, subsequently, their nuclei equal the charge distribution of the excited molecule. Besides redistribution of electron orbitals (dielectric relaxation) this may include the shifts of solvent nuclei and reorientation of solvent molecules as dipoles. Dielectric relaxation is near immediate effect, faster than 10 fs. Environment molecules rearrangement is called solvation; its rate depends on the solvent molecules mobility and their dipole moments. Generally, they occur in the range of picoseconds and tens of

picoseconds. Obviously, when solvation takes place the energy of the excited state must decrease. The ground state energy shows the environment is now adjusted to the excited state. At this stage, the energy of the ground state would be higher than that of a relaxed ground state. It is stated that, as shown in figure 15 (A) solvation reduces the energy of the excited state and increases to the ground state. By the stimulated emission spectrum, the energy gap between these states is directly measured. Therefore, as shown in figure 15 (B) maximum stimulated emission will shift towards the red upon solvation. Ground state bleaching spectrum will not be sensitive to solvation; it represents the absorption that disappeared upon excitation, therefore it will stay in place. When the molecule returns to the lowest energy ground state, this absorption disappears at the time constant of excitation and is recovered.

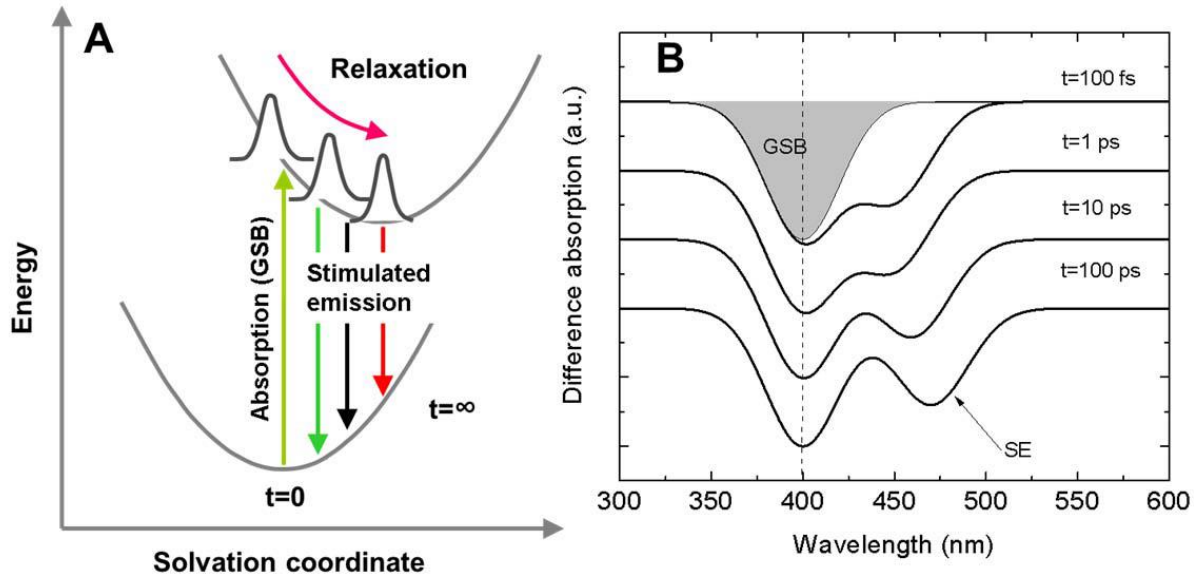

Figure 15. (A) Potential energy surfaces for solvation: when the molecule is excited, the environment reorients to fit the new electronic configuration of the solute. This leads to the decrease of the excited state energy and the increase of ground state energy. As a result, SE spectrum observed in a transient absorption experiment, shifts to the red (B). The GSB spectrum remains unaffected. [45]

5.5.5.3 Conformational change of the molecule

Light induced change in molecular structure is another reaction. There are many types of conformational change, among that trans-cis isomerization is the one example. Because of their potential applications in nanotechnology, optoelectronics, information storage, etc., the molecules able to undergo conformational changes under light excitation is interesting. In this section, it is discussed that the changes of the transient absorption spectrum result from the isomerization of the molecule. As in the case of solvation, the excited and ground state energies will follow the same general trend. Stimulated emission signal shifting towards the red is expected. Stimulated emission will disappear, after the completion of isomerization and return to a new ground state, because there will be no more excited state able to emit photons. However, from the originally excited state, the ground state will be different. Therefore, we can expect that some ground state bleaching will still exist and there will be new induced absorption contribution matching the energy gap between the new ground state and its excited state. It is summarised that, transient absorption spectroscopy allows us to observe not only the course of photo-isomerization, but also the absorption of the product being formed.

5.5.5.4 Formation of a triplet state

Similarly, to a conformational change, other photo-induced transformations of a molecule, such as triplet state formation can be analysed. As compared to the singlet excited states, triplets hardly emit any light, therefore, stimulated emission signal in transient absorption spectrum will disappear, after intersystem crossing, and the induced absorption of triplet state will become visible. Until the formed triplet state decays, the ground state bleaching signal will persist.

5.5.5.5 Excitation energy transfer

Excitation energy transfer can be monitored by many type of spectroscopies like transient absorption spectroscopy. Transient absorption signatures (GSB, SE and IA) will disappear and be replaced by the difference absorption spectrum of excited acceptor, when donor molecule transfers the excitation energy to the acceptor molecule. To monitor the energy transfer between molecules with femtosecond time resolution, transient absorption spectroscopy is an excellent tool. By comparing to another spectroscopy like time-resolved fluorescence spectroscopy, where femtosecond resolution is only available in fluorescence up conversion experiments; transient absorption spectroscopy is more sensitive, provides better signal-to noise ratio, also more flexible, because donor and acceptor populations can be observed at different wavelengths. For example, at donor excited state absorption and acceptor bleach wavelengths. Experiment sensitivity and selectivity of transient absorption spectroscopy can be increased, by selecting the spectral bands appropriately.

5.5.5.6 Proton or electron transfer

Relates to the photo-induced charge transfer events, Proton or electron transfer is very important class of photo-induced reactions. Transfer of proton occurs in molecules called photo-acids and Photo-bases. Proton or electron are molecules with easily protonating groups (for example, –OH), the pK_a of the molecules changes upon excitation. There are two types of proton transfer are possible: proton dissociation, when the proton goes to the environment leaving behind a molecular anion, and intramolecular, when the proton leaves one group of the molecule and attaches to another group. Formation to two radicals of both molecules occurs, when electron transfer occurs between electron donor (the molecule which receives excitation) and acceptor. Proton or electron transfer on the physical basis is always the same: the excited molecule can reduce its energy by releasing or capturing proton or electron. The donor molecule returns to the ground state, when this charge carrier is caught and stabilized by the molecules in the environment, which could be solvent or acceptor molecules; but the charge is not available anymore, because it is bound to the environment molecules. Therefore, the system remains in the charge-separated state, at least for some time, including radical, ion or isomer. The molecules acquire a net electric charge, because all these reactions are inevitably accompanied by structural changes in the molecule. Therefore, change in the absorption spectrum is necessarily reflected. To analysing the transient absorption signals, we may expect that initially, at short delay times we will observe the spectrum of the excited donor, where is excited states are easy to discern by their stimulated emission signals. Corresponding to the acceptor radical, this signal will decay and be replaced by new absorption bands. It is stated that, the ground state bleaching of the donor will also remain, rather than returning to its original ground state, because the donor will have become a radical too. In summary, we can expect to observe the following, when charge transfer is complete: a) donor ground state

bleaching; b) donor radical induced absorption (or ion induced absorption); c) acceptor ground state bleaching; d) acceptor radical induced absorption (or ion induced absorption).

5.5.5.7 Photoionization

Photoionization is the another group of photo-induced events visible in transient absorption experiments. The photon will rip off an electron from the molecule, if the energy of absorbed light quantum is higher than the ionization potential of the molecule; this electron will be ejected into the environment. We will not be able to observe the excited state of the molecule, as this process is instantaneous. Instead of that, the excitation will instantly result in the spectrum composed molecular ground state bleaching and radical induced absorption. We will also observe the induced absorption spectrum of solvated electron, that is electron surrounded by oriented solvent molecules; if the molecule is dissolved in liquid or embedded in solid-state matrix. Induced absorption band is very broad, its width is around 0.84 eV, and has a maximum at roughly 720 nm in water. It is stated that, when the peak power of excitation pulse is high in ultrafast experiments, photoionization may also be induced by multi-photon absorption. Because the energy of two photons is combined to ionize the molecule**,** the wavelength of the pump pulse may be longer than the photoionization threshold of the molecule.

6. Aim of this study

Ultrafast phenomena are very tough to handle even using light, as it is much faster. Therefore, in order to investigate them, light needs to be controlled in an especially precise manner. Several light properties should have reached to be in perfection, for example, Intensity, Color (Wavelength), Direction, Duration of Pulse (flash), Polarization, Phase etc.

Transient absorption spectroscopy (TAS) is a very useful and powerful technique to directly observed time resolved absorption spectra of photo-generated charge carriers (electron and holes) in nanomaterials, and knowledge of the carrier dynamics drawn from TAS gives appropriate characterization of material properties and selection of proper applications. In the measurement at the time scale of femto to nanoseconds, time resolved measurement is made possible by using short pulsed light for both pump light and probe light.

In this study, ultrafast carrier dynamics of laser-ablated graphite and reduced graphene oxide with metal composites is measured by using femtosecond transient absorption spectroscopy.

Chapter 2. Experimental

1. Sample preparation

1.1 Preparation of rGO

Graphite powder (>20 μm size), H_2SO_4, $NaNO_3$, NaOH, H_2O_2 (30%), $K_3Fe(CN)_6$ and $KMnO_4$ were purchased from Sigma-Aldrich Co., 3050 Spruce street, St. Louis, MO 63103 USA. All the chemicals are used as received without further purifications. GO was prepared from graphite powder using modified version of Hummers method [16]. Graphite powder (1 g) and sodium nitrate (0.5 g) were mixed together followed by the addition of conc. sulphuric acid (23 ml) under the constant stirring. After 1 hour, $KMnO_4$ (3 g) was added to the above solution gradually. To prevent explosion and overheating, temperature is maintained less than 20°C. Further, the mixture was stirred at 35°C for 12 hours and 500 ml of water was added under vigorous stirring in the resulting solution. The suspension was treated with 30% H_2O_2 solution (5 ml), to ensure the completion of reaction with $KMnO_4$. The mixture was further washed with HCl and H_2O respectively. The resulting solution was filtered and dried to get the graphene oxide (GO) powder. The thermal reduction of GO was carried out in a quartz tube at 1050°C under Ar gas ambience for 30-minute duration. The GO was completely converted into reduced graphene oxide (rGO).

1.2 Preparation of rGO-metal (Au, Pd & Pt) Composites

rGO-Au composite: rGO (10 mg) was dispersed via sonication in 30 mL of DMF-water solution. $AuCl_3 \cdot HCl \cdot H_2O$ (6.3 mg) was added and then stirred for 1 hour. The freshly prepared $NaBH_4$ aqueous solution (0.118 M) was added into the mixture. The mixture was heated at 80 °C for 4 hours. The product washed with ethanol.

rGO-Pd composite: rGO (10 mg) was dispersed via sonication in 20 mL of ethylene glycol-water solution. $PdCl_2$ (12.8 mg) was added and the mixture was heated at 125 °C for 4 h. The product washed with ethanol.

rGO-Pt composite: rGO (10 mg) was dispersed via sonication in 20 mL of ethylene glycol-water solution. K_2PtCl_4 (6.4 mg) was added and the mixture was heated at 125 °C for 4 hours. The product washed with ethanol.

2. Laser ablation

Figure 16 is a schematic of the nanoparticle formation process by laser ablation. When the laser beam is focused on the surface of a solid target material in the ambient media (gas or liquid), the temperature of the irradiated spot rapidly increases, vaporizing the target material. The collisions between the evaporated species (atom and clusters) and the surrounding molecules result in excitation of the electron state coupled with light emission and generation of electrons and ions, forming a laser-induced plasma plume. The plasma structures (size of the plume and its emission spectrum) depend on the target material, ambient media (liquid or gas), ambient pressure, and laser conditions. Laser ablation in liquid is employed to confine the plasma plume in a small region to directly disperse nanoparticles in the liquid phase [46].

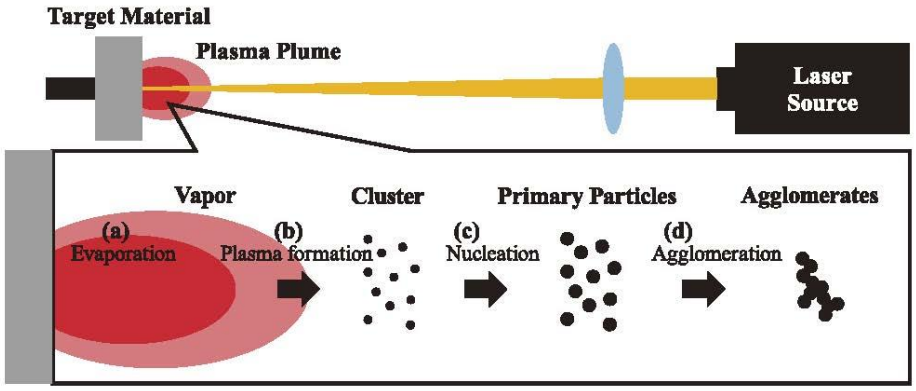

Figure 16. Schematic of particle generation procedure in the laser ablation process. [36]

Figure 17. shows experimental set-up of laser ablation. The solution of graphite powder (200 mg) and acetone (20 mL) were mixed in a glass bottle. The laser ablation was carried out under magnetic stirring. The laser pulses generated from the second harmonic of a Nd:YAG (Yttrium Aluminium Garnet) laser (wavelength 532 nm, repetition frequency 10 Hz, 10 ns fwhm, 55 mJ pulse^{-1}, Spectra Physics Quanta-Ray) have been used for laser ablation.

The laser ablation time was 240 minute with the solution being continuously stirred by a magnetic rotor during irradiation. The size of laser beam was about 5 mm in diameter. After laser ablation, solution was cooled at room temperature. Then the solution was heated at 90 °C to evaporate the acetone and get the dry sample in powder form for characterization.

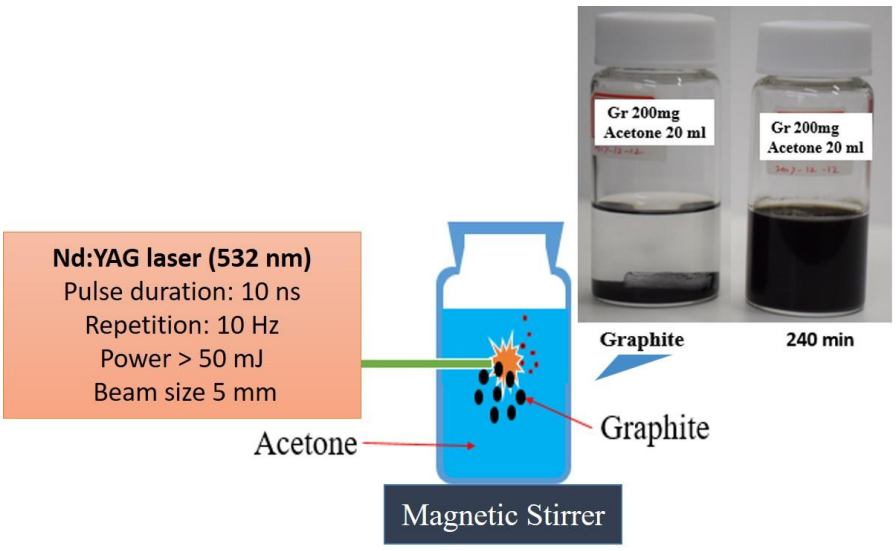

Figure 17. Experimental set-up of laser ablation.

3. Characterization methods

Ultraviolet-visible (UV-vis) absorption spectra of the graphite, laser-ablated graphite, rGO and rGO with Au, Pd and Pd were obtained with the ultraviolet-visible absorption spectrometer (JASCO, V-670).

The morphology of graphite, laser-ablated graphite, rGO with Au, Pd and Pd was observed under scanning electron microscope (SEM, S-4700, Hitachi).

Raman spectroscopy analysis of graphite and laser-ablated graphite was performed using confocal micro-Raman LabRAM HR evolution Raman microscope (Horiba) with 532 nm laser.

X-ray diffraction analysis (XRD) of the graphite and laser-ablated graphite was carried out on Bruker AXSD-8 Advance X-ray diffractometer with monochromatic CuKα, radiation (λ=1.5406 A°). Data were collected from 10° to 80° at a scan rate of 0.1° min-1.

4. Femtosecond transient absorption spectroscopy (fs-TAS)

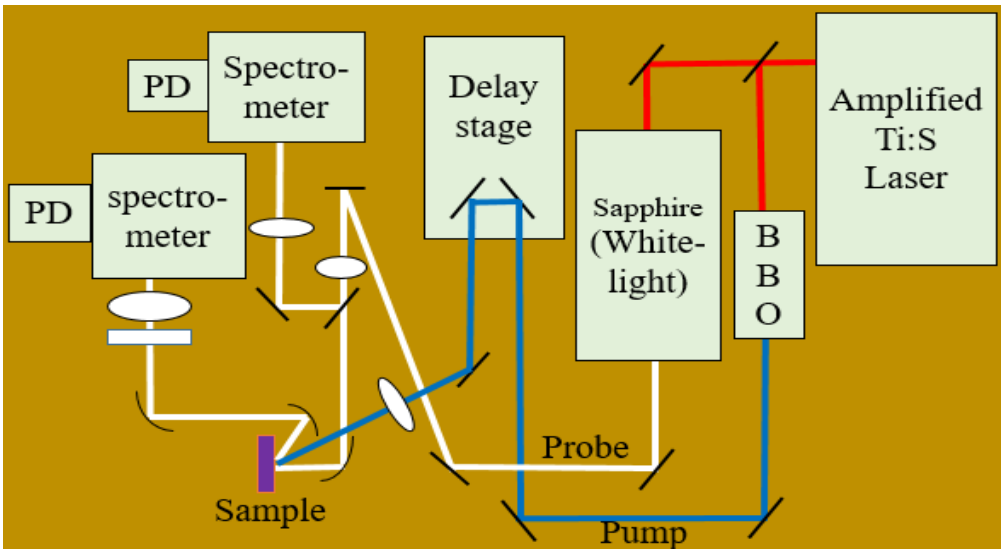

Figure 18. Optical set-up of fs-TAS at diffuse reflection system.

Figure 18 shows optical set-up of femtosecond transient absorption spectroscopy at diffuse reflection system. Ultrafast carrier dynamics of graphite, laser-ablated graphite, rGO and rGO with Au, Pd and Pd, is measured using fs-TAS. The light source for transient absorption spectroscopy was a femtosecond titanium sapphire laser with a regenerative amplifier (Hurricane, Spectra Physics, 800 nm wavelength, 130 fs fwhm pulse width, 0.8 mJ pulse^{-1}, 1 kHz repetition). The fundamental beam was split into two and one of them was used as pump light after converting to the second harmonic of 400 nm wavelength at a 500 Hz modulation frequency. The other beam was used as probe light after converting to the white-light continuum by focusing the fundamental beam into a sapphire plate (2 mm thick). At the centre of the pump light (~0.3 mm diameter) the probe light was focused on the sample. The diffuse reflected probe light from the sample was detected by the Si photodiode after passing through a monochromator (Acton Research, SpectraPro-150). TA intensity was evaluated as %Abs. = $100(R_0-R)/R_0$, where R_0 and R were diffuse reflected probe light intensity without and with excitation, respectively [47].

5. Photocatalysis

Figure 19 shows set-up of photocatalysis experiment. Photocatalysis activity of rGO with Au, Pd and Pt was carried out using Methylene blue dye as a degradation component. 1.5 mg of Methylene blue is added in 125 ml distilled water and 1 mg of each sample is added in the mixed solution. Two types of light sources are used, one is Xenon white lamp and another is blue LED. The solution is continuously stirred by magnetic stirrer and stirrer bar. For every 10 minutes of time interval solution is taken for UV-vision absorption measurement, for analysis of the decrease in absorption intensity of each sample.

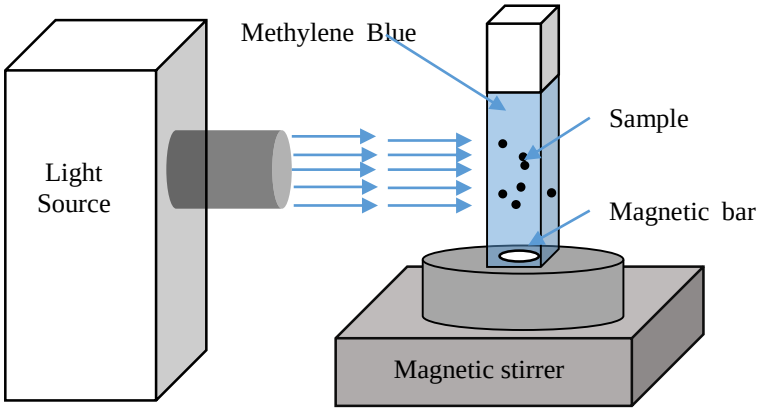

Figure 19. Set-up of photocatalysis experiment.

Chapter 3. Characterization Results

1. Ultraviolet-visible (UV-vis) absorption analysis

To evaluate the optical absorption nature of the opaque solid specimens dispersed in fluids, UV-Vis absorption spectroscopy was used. 10 mg graphite powder was added into 10 ml of acetone. 10 mg laser-ablated graphite powder was added into 10 ml of acetone. 10 mg of rGO was added into the mixed solvent of 7 ml distilled water and 3 ml methanol. In Figure 20, graphite and laser-ablated graphite show the absorption peaks same at 274 nm [48], while only the absorption intensity increased after ablation. On the other hand, the absorption peak of the rGO shifts to 267 nm [49], corresponding to the thermal reduction of graphene oxide produced by hummers method. The absorption rise toward 200 nm in original and ablated graphite samples are seen. These are the effects of acetone used as a solvent. Although light scattering by the particle nature gives an offset to absorbance, it seems the main optical property of graphite remains unchanged even after the laser ablation treatment.

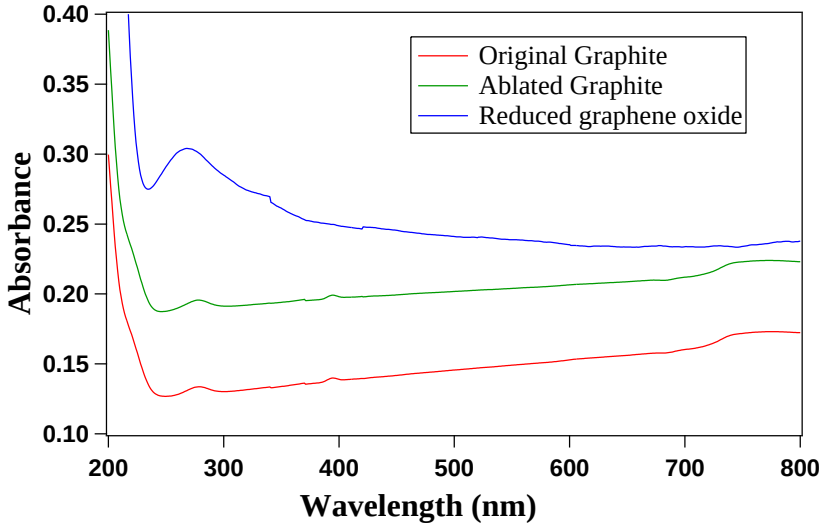

Figure 20. UV-Vis spectrum of graphite, laser-ablated graphite and rGO.

UV-Vis spectra of rGO with Au, Pd and Pt are shown in figure 21. 10 mg of each rGO-metal sample was added into 10 ml distilled water for UV-Vis absorption analysis. The characteristic surface plasmon resonance (SPR) absorption peak of Au observed in rGO-Au sample at 530 nm. Along with rGO absorption peak at 267 nm, it is confirmed that rGO-Au composite formed successfully [50]. rGO-Pd sample exhibited a characteristic surface plasmon resonance absorption band at 300 nm and followed the absorption band in visible region. Along with rGO absorption peak about 267 nm it is confirmed that rGO-Pd composite formed successfully [51]. In rGO-Pt absorption spectra, absorption in UV region with the rGO peak about 270 nm confirmed that rGO-Pt composite also formed successfully [52].

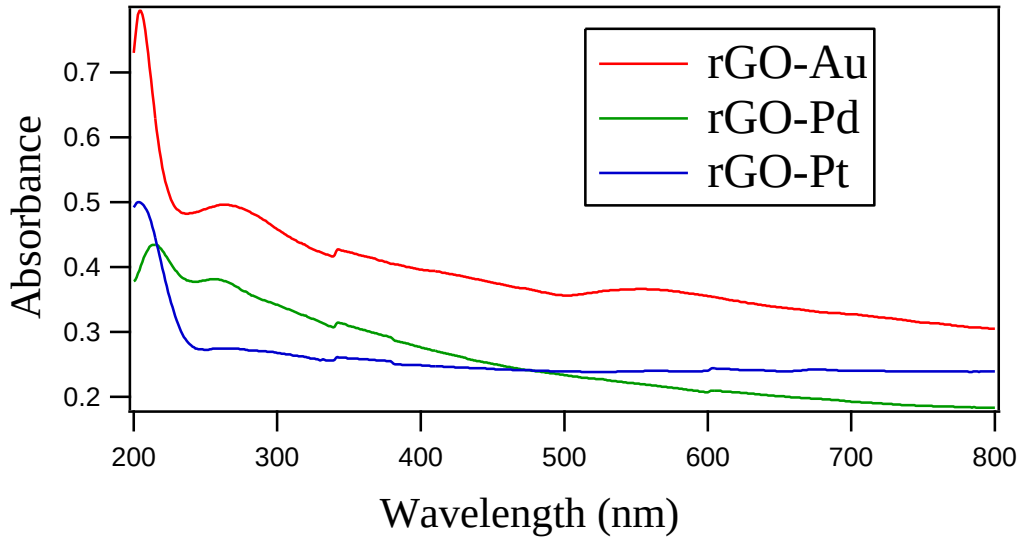

Figure 21. UV-Vis spectrum of rGO with Au, Pd and Pt.

2. Scanning electron microscopy analysis

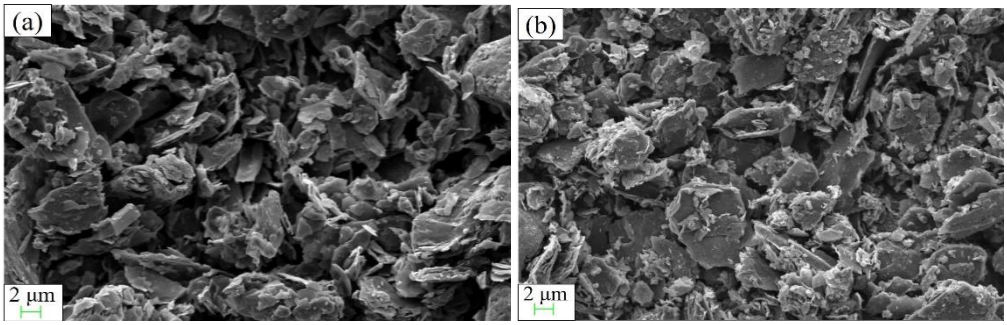

Figure 22. SEM Images of graphite (a) before ablation and (b) after ablation.

In scanning electron microscopy, by using electron beam surface of the specimen is analysed. Figure 22 (a) shows SEM image of the graphite before ablation. The surface of graphite is found to have a layered structure [53] and some ununiformed layers in the original graphite powder. Figure 22 (b) shows SEM image of graphite after 240 min laser ablation, in which composed overlapping graphite thin layers are formed. This structure clearly shows the effect of laser ablation.

Figure 23 (a) Shows SEM image of rGO-Au nanoparticles. The uniform distribution of spherical Au nanoparticles on the surface of rGO was clearly observed [54]. rGO layers are also clearly observed in the structure. Figure 23 (b) shows SEM image of rGO-Pd nanoparticles. rGO sheets are also clearly observed on a several nm, it shows that Pd nanoparticles are well distributed on rGO [55]. Figure 23 (c) shows SEM image of rGO-Pt nanoparticles. rGO sheets shows wrinkle paper like structure. Pt nanoparticles are clearly observed on the rGO layers [56].

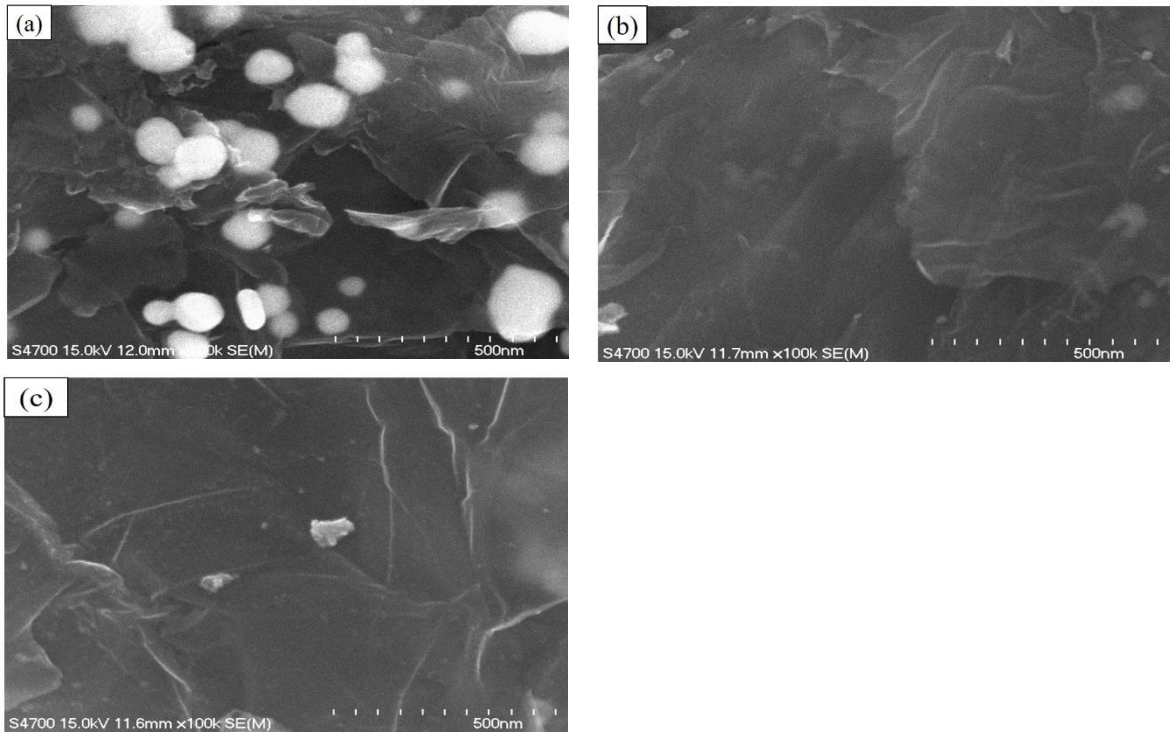

Figure 23. SEM Images of (a) rGO-Au, (b) rGO-Pd and (c) rGO-Pt.

3. Raman spectral analysis

Raman spectroscopy is an essential tool for characterization for carbon based materials, and the spectrum is highly sensitive to the lattice and electronic structures. Raman spectroscopy analysis was carried out for original graphite and laser ablated graphite. In figure 24, the band observed at about 1577 cm^{-1} shows G-band, which corresponds to a splitting of the E_{2g} stretching mode of graphite and reflects the structural intensity of the sp^2-hybridized carbon atom. D-band appears at 1350 cm^{-1}, assigned to zone center phonons of K-point phonons of A_{1g} symmetry, characterizes the disordered graphite planes and the defects incorporated into heptagon and pentagon graphitic structures. G´-band at 2712 cm^{-1} is related to the intrinsic property of well-ordered sp^2 carbon structures for graphite [57]. After laser ablation, D-band and G´-band peaks are slightly shifted to right side by 5-10 wave numbers, but there is no obvious change in peak position for G-band. However, the G/D ratio decreases from 4.13 to 3.38, indicating the edge effect in laser ablated nanostructures. In our group, under the same experimental set-up, laser ablation of MoS_2 shows change in peak position in Raman spectra [58].

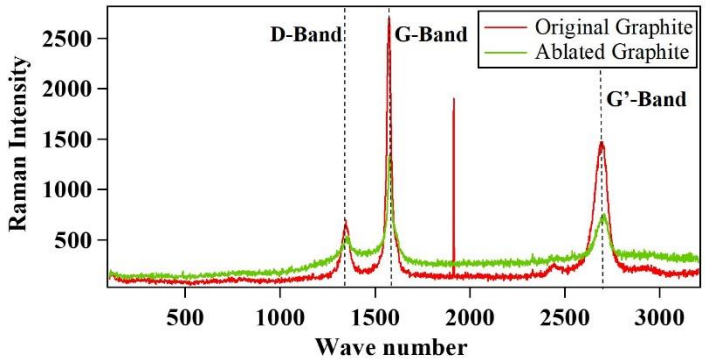

Figure 24. Raman spectra of graphite and laser ablated graphite.

4. X-ray diffraction (XRD) analysis

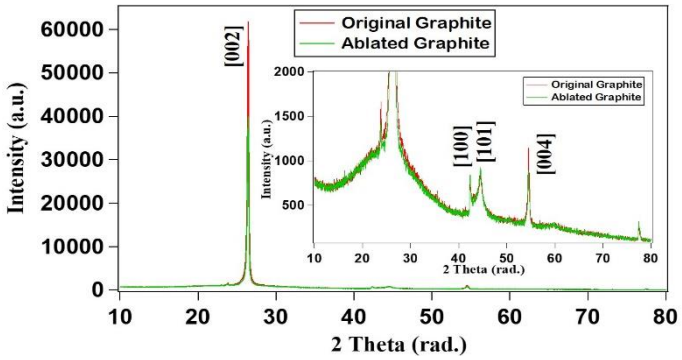

Figure 25. X-ray diffraction patterns of graphite and laser-ablated graphite.

XRD was used for the determination of lattice parameters and the crystal structure. In Figure 25, we observed peak (002) at the plane ($2\theta = 26°$) of original graphite powder. In the zoom image, we observed the normal peaks (100), (101), (004) at the plane ($2\theta = 43°,46°,55°$) in Cu anode (and corresponding to 31°, 50°, 52°, 64° peaks for Co anode respectively) [57]. After the laser ablation for 240 min, peaks at 26° and 55° that are assigned to (002) and (004) layers of graphite, stipulate the formation of graphitic nature which indicates it is not an amorphous structure. Narrow FWHM (Full width and half maximum) of (002) peak appears from the continuity of graphene layers, the broadness of this peak in the carbon soot originates from the random distribution of the basic structure. The lack of intensity in the other graphite peaks in XRD patterns shows that there are fewer groups of lattice planes in the laser ablated graphite structure compared to the original graphite structure. The fragmentation of the structure to smaller pieces can be concluded, but no change in peak positions indicating that the graphite is hard and stable material in the case of structural properties. In our group, under the same experimental set-up, laser ablation of boron nitride shows change in peak position in XRD patterns [59].

Chapter 4. Ultrafast Carrier Dynamics

1. Carrier dynamics of graphite, laser-ablated graphite and rGO

As shown in figure 26, a prompt absorption rise was clearly observed in femtosecond transient absorption time-profiles of the graphite. After prompt absorption rise, graphite shows decay about 300±20 fs. This fs decay is obtained due to intra-band relaxation of the excited electrons [60]. In figure 26 (a), highest absorption intensity is observed at 850 nm probe wavelength as we experimented different probe wavelengths among 700 nm to 1000 nm. The spectrum is shown in the inset of Figure 26 (a). Also, we have experimented different pump fluence dependence spectra. Figure 26 (b) shows TA peak intensity with 0.25 mJ/cm^2 pump fluence is most strong with stable optical response among 0.0625 mJ/cm^2 to 0.4375 mJ/cm^2. At 0.25 mJ/cm^2 pump fluence, peak absorption started saturating as the dependence is shown in the inset of Figure 26 (b). An inter-band transition is an electronic transition between a lower filled band and an upper band. Photo-excitation is known to cause a bleaching of this transition. This phenomenon appears as the initial response with a small negative dip at time zero. An intra-band transition is a transition between electronic states within the conduction band. This contribution becomes dominant as a positive optical response is observed [60]. The decay process reflects cooling of thermally excited electrons near the Fermi level (the Dirac point in the case of rGO). An energy scheme for graphite is shown for the optical transitions of excitation (at 400 nm) and probe (at 850 nm) in Scheme 3.

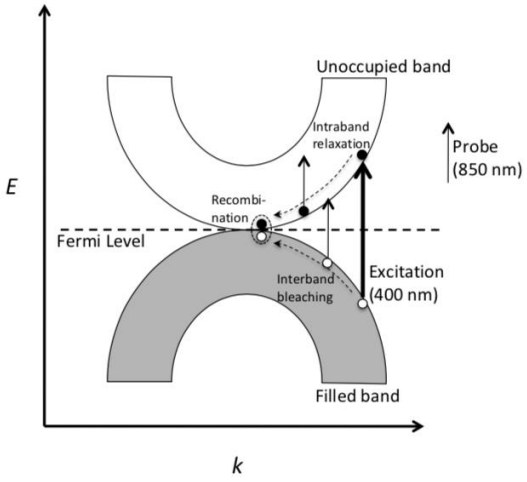

Scheme 3. Energy scheme for graphite for the optical transitions of excitation (at 400 nm) and probe (at 850 nm)

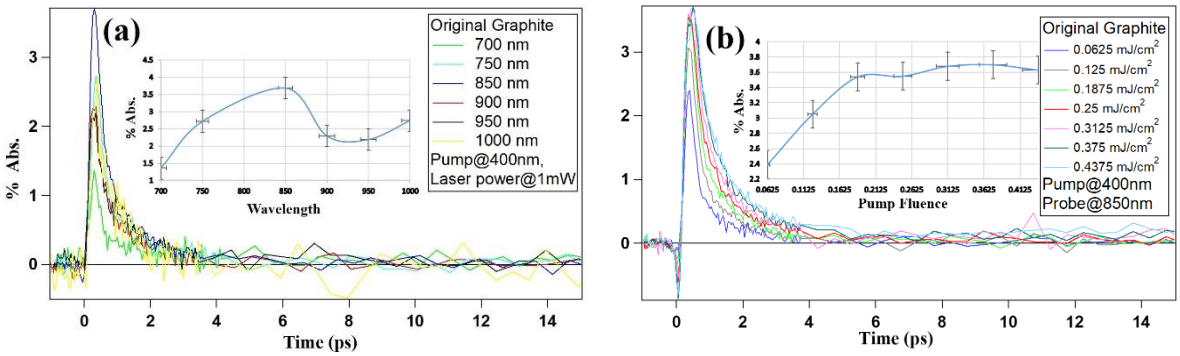

Figure 26. Transient absorption spectra of graphite (a) wavelength dependence and (b) Pump fluence dependence.

Comparison of transient absorption spectra of graphite, laser-ablated graphite, and reduced graphene oxide (rGO) is experimented with 850 nm probe wavelength and pump fluence of 0.25 mJ/cm^2. In figure 27, we notice that normalized transient absorption spectra of all three samples give similar dynamics, in which the decay after the prompt excitation is composed of an ultrafast component for original graphite at 287 fs, laser-ablated graphite at 309 fs and rGO at 260 fs. The result shows ..

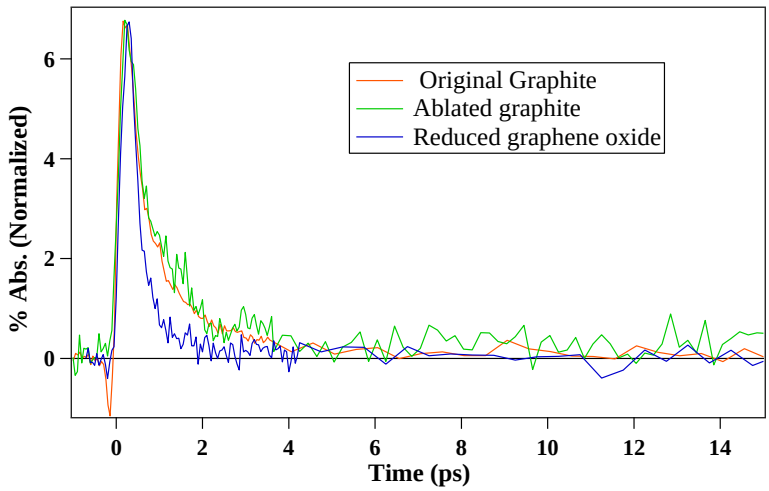

Figure 27. Comparison of transient absorption spectra of graphite, laser-ablated graphite and rGO.

These decay profiles are analysed using a double exponential function (Table 4).

$A_1\exp(-t/\tau_1) + A_2\exp(-t/\tau_2) + C$

Focusing on τ_1, this parameter of rGO is smaller compared to graphite before ablation and after ablation. In the slow component, τ_2, graphite before and after ablation are smaller than rGO. Figure 27 shows that the decay times are only a few hundreds of fs for graphite and rGO. Therefore, at these pump/probe wavelengths the ultrafast response is suitable for developing the femtosecond optical switches.

Table 4. Fitting parameters of TA decay of graphite, laser-ablated graphite and rGO.

	A_1	τ_1 (ps)	A_2	τ_2 (ps)	C	% Abs.
Original graphite	1.935±0.181	0.287±0.0293	1.594±0.189	1.122±0.088	0.093	3.5
Ablated graphite	1.504±0.639	0.309±0.12	1.946±0.666	1.019±0.199	0.158	3.5
rGO	6.659±0.186	0.26009±0.0114	0.466±0.151	2.5208±1.39	0.005	6.7

2. Carrier dynamics of rGO with Au, Pd and Pt composites

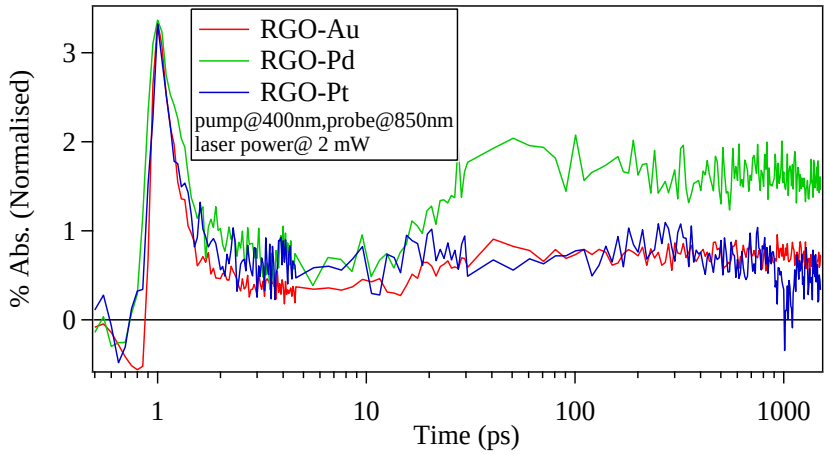

Figure 28. Comparison of transient absorption spectra of rGO with Au, Pd and Pt.

Comparison of transient absorption spectra of rGO with Au, Pd and Pt is experimented with 850 nm probe wavelength and pump fluence of 0.25 mJ/cm^2. In figure 28, we notice that normalized transient absorption spectra of all three samples give similar dynamics, in which the decay after the prompt excitation is composed of an ultrafast component for rGO-Au at 226 fs, rGO-Pd at 304 fs, rGO-Pt at 177 fs. After the prompt excitation and decay all three samples shows long lived component up to the 1000 ps. Au, Pd and Pt (Metals) transfers the electrons to the rGO which may be the possible candidate for the long lived component (Scheme 4).

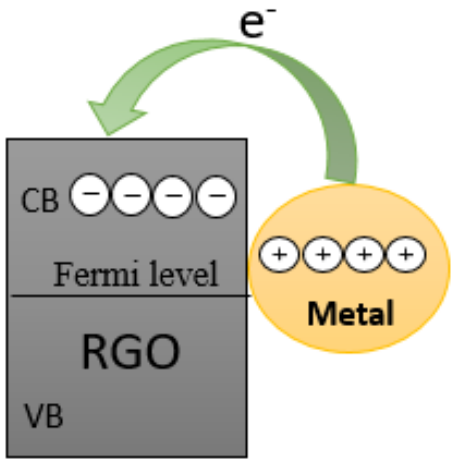

Scheme 4. Energy scheme for Metal to rGO electron transition.

The decay profiles are analysed using a triple exponential function (Table 5).

$A_1\exp(-t/\tau_1) + A_2\exp(-t/\tau_2) + A_3\exp(-t/\tau_3) + C$

Table 5. Fitting parameters of TA decay of rGO with Au, Pd and Pt.

	A_1	τ_1 (ps)	A_2	τ_2 (ps)	A_3	τ_3 (ps)	C
rGO-Au	2.364± 0.087	0.226± 0.01	0.777± 0.268	3.921± 1.42	-1.017± 0.256	19.697± 6.87	0.938± 0.06
rGO-Pd	1.604± 0.107	0.304 ± 0.0408	1.660± 2.77	5.383± 4.16	-2.164± 2.82	11.933± 6.3	1.173± 0.03
rGO-Pt	1.782± 0.26	0.177± 0.04	0.503± 0.26	0.972± 0.46	-	-	1.4

Chapter 5. Photocatalysis Activity

1. Photocatalysis of rGO with Au, Pd and Pt composites

1.1 Photocatalysis activity using Xenon white lamp

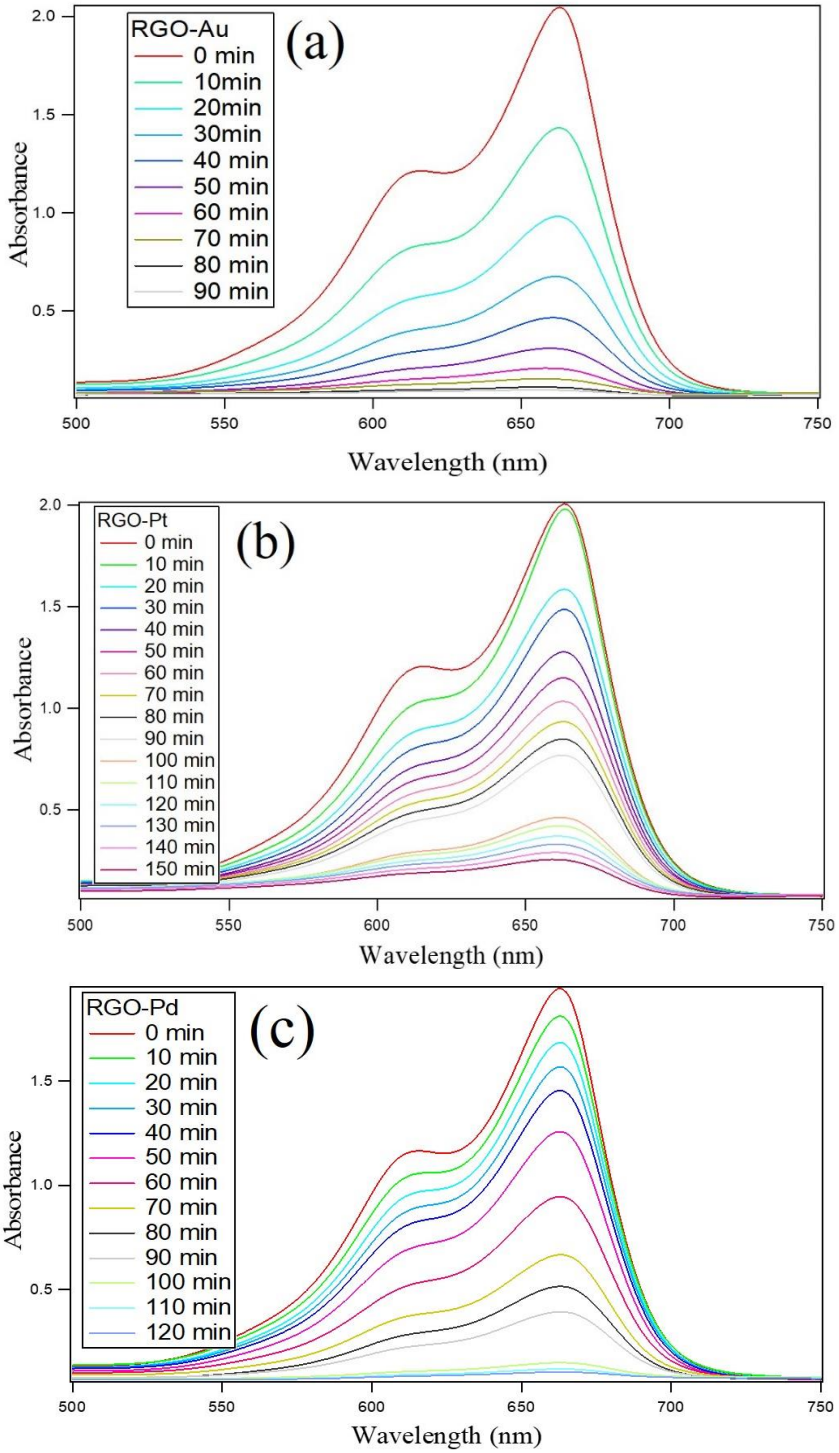

Figure 29. UV-vis spectrum of photocatalysis degradation using Xenon white lamp (a) rGO-Au, (b) rGO-Pt and (c) rGO-Pd.

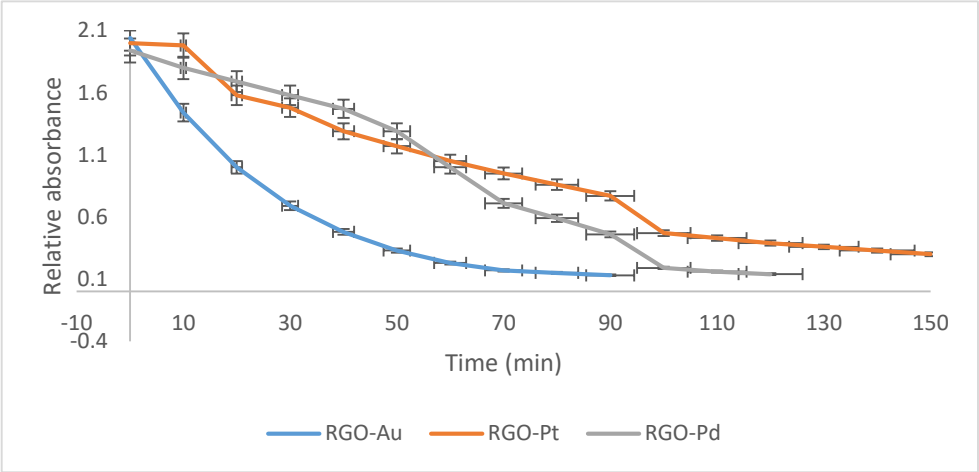

Figure 30. Relative absorbance comparison of rGO with Au, Pd and Pt using Xenon white lamp.

Xenon white lamp excites in the visible region. Figure 29 shows UV-vis spectrum of photocatalysis degradation of (a) rGO-Au, (b) rGO-Pt and (c) rGO-Pd. Figure 30 shows the relative absorbance of rGO with Au, Pd and Pt. It shows rGO-Au degrades the methylene blue faster in 90 minutes while rGO-Pd degrades in 120 minute and rGO-Pt takes more than 150 minutes. rGO-Au shows faster degradation tendency because of Au nanoparticle shows surface plasmon resonance absorption in visible region about 520 nm wavelength [62].

1.2 Photocatalysis activity using Blue LED

Blue LED excites in the Ultra-violet region at 368 nm wavelength. Figure 31 shows UV-vis spectrum of photocatalysis degradation of (a) rGO-Au, (b) rGO-Pt and (c) rGO-Pd. Figure 32 shows the relative absorbance of rGO with Au, Pd and Pt. It also shows rGO-Au degrades the methylene blue faster in 90 minutes while rGO-Pd and rGO-Pt shows slower degradation rate than the rGO-Au. In Ultra-violet region also rGO-Au shows faster degradation tendency because Au nanoparticle shows inter-band excitation in ultra-violet region about 400 nm wavelength [62].

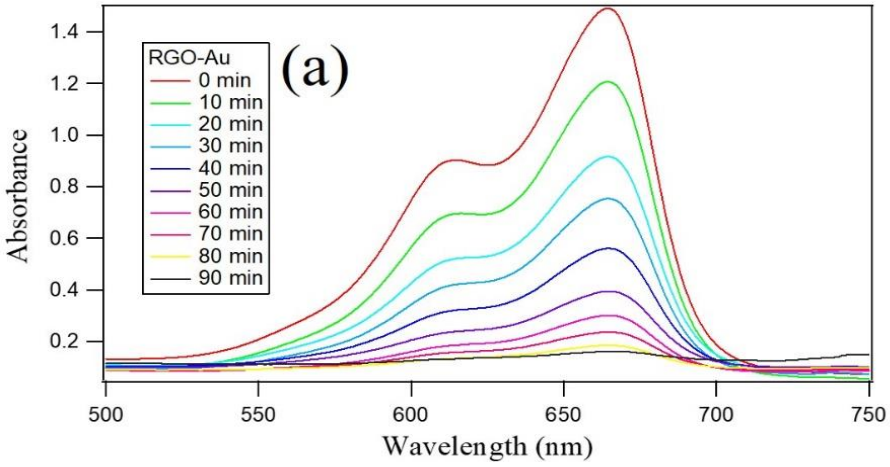

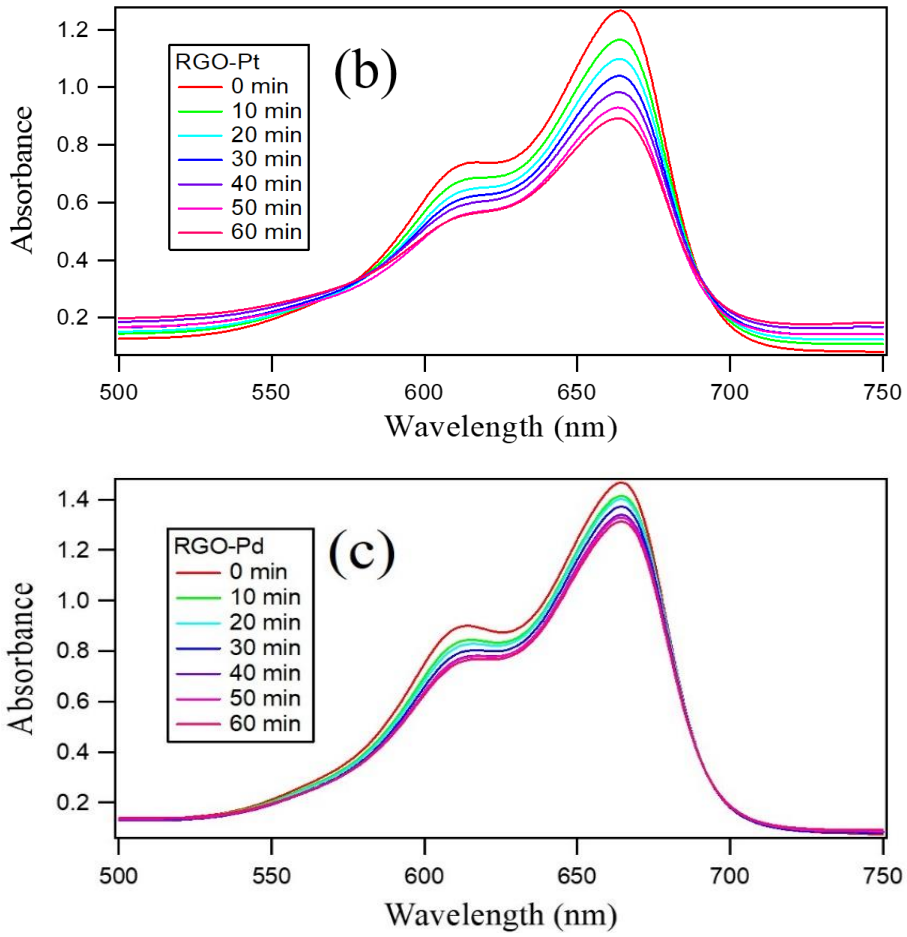

Figure 31. UV-vis spectrum of photocatalysis degradation using Blue LED (a) rGO-Au, (b) rGO-Pt and (c) rGO-Pd.

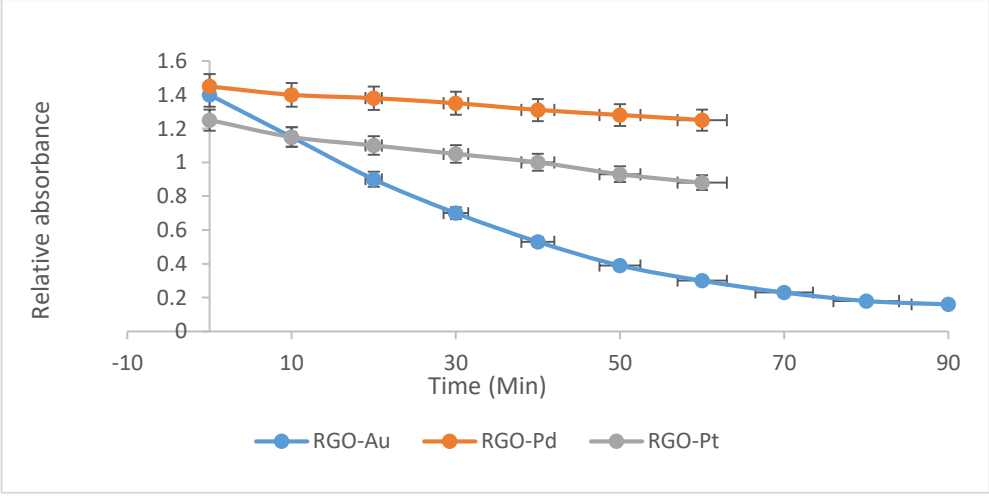

Figure 32. Relative absorbance comparison of rGO with Au, Pd and Pt using blue LED.

Figure 33 describes UV-Visible absorption spectra of rGO-Au composite. Surface plasmon resonance (SPR) absorption of Au nanoparticle is clearly observed about 520 nm wavelength. On the other hand, inter-band excitation in ultra-violet region about 400 nm wavelength is seen. These two important properties are advantageous in the faster degradation of rGO-Au composite for the photocatalytic activity.

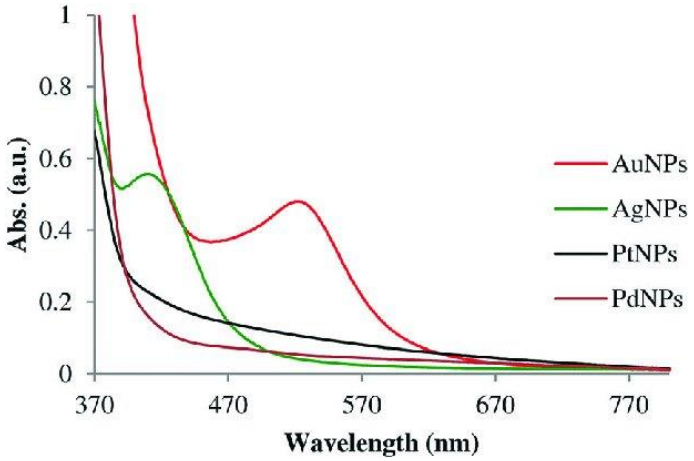

Figure 33. UV-Vis spectrum of rGO with Au, Pd and Pt. [62]

In Addition to rGO-metal composites, photocatalysis activity of TiO_2 is performed in methylene blue. Xenon lamp is used as a light source. TiO_2 seems to be a good catalyst than rGO-metal composites. It decomposes the methylene blue in 10 minutes. Figure 34 shows the UV-vis spectrum of photocatalysis degradation of TiO_2, from 0 to 10 minutes. The 10-minute sample totally converted from blue color to white color. Without using the light source, adsorption of sample is also measured, but the absorbance decays very slightly as shows in the figure.

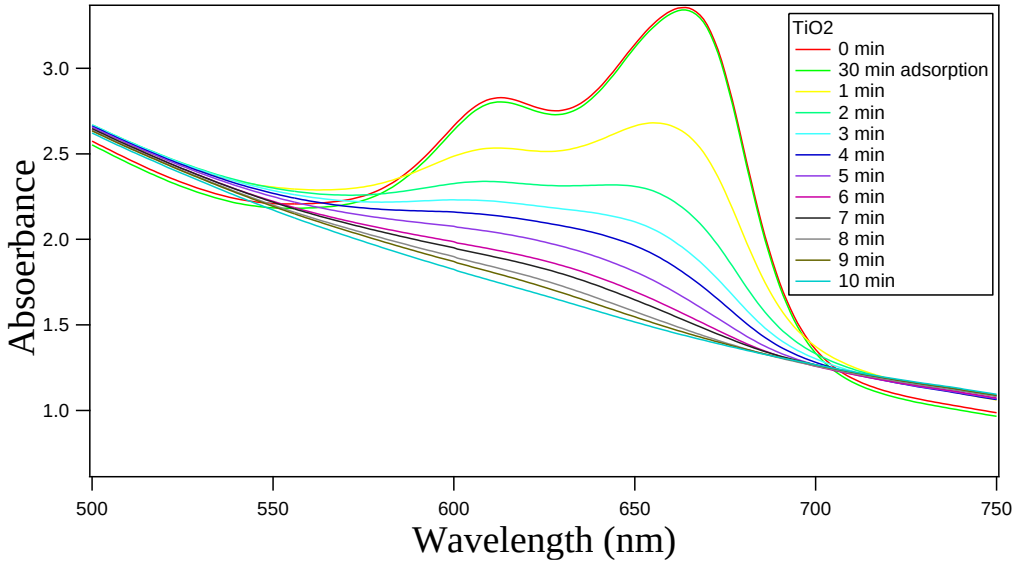

Figure 34. UV-vis spectrum of photocatalysis degradation of TiO_2 using Xenon lamp

Chapter 6. Summary

Graphite was laser-ablated for 240 minute and we have compared the results of graphite and laser-ablated graphite through different characterization techniques. Reduced graphene oxide (rGO) was synthesized by modified Hummers method and reduced it by thermal reduction method. Au, Pd and Pt are decorated on rGO by chemical synthesis. UV-Vis spectrum confirmed the peaks of both graphite (non-ablated and laser-ablated) and rGO at 274 nm and 267 nm respectively. It also confirms the synthesis of rGO with Au, Pd and Pt composites successfully. SEM image displayed the overlapping layered structure in laser-ablated graphite. SEM images of rGO with Au, Pd and Pt shows successful compositions of Au, Pd and Pt on rGO nanosheets. XRD and Raman spectroscopy showed the peak intensities decreased after laser ablation.

Femtosecond transient absorption spectroscopy confirmed the ultrafast excitation and relaxation of graphite, laser-ablated graphite, and rGO. The carrier relaxation occurred for graphite at 287 fs, laser-ablated graphite at 309 fs and for rGO 260 fs. rGO shows TA intensity about 6.7%, while both graphite samples showed 3.5%. Although rGO shows higher absorption intensity than both graphite samples, much cheaper graphite is also useful for the future application of optical switching. In future, another material can be used with graphite as a composite material to achieve enhanced TA intensity. It will be the better way to achieve optical switching application while saving the cost of the material.

Photocatalysis activity shows faster degradation of methylene blue for rGO-Au composite in 90 minutes using both xenon white lamp and blue LED. rGO-Pd composite takes 120 minute while rGO-Pt composite takes 120 minute for degradation of methylene blue using xenon white lamp. Also, using blue LED both rGO-Pd composite and rGO-Pt composite shows slower degradation rate than rGO-Au composite. rGO-Au composite is useful composition for the photocatalysis activity. rGO with Au, Pd and Pt shows similar dynamics with long lived component in ultrafast carrier dynamics. The faster degradation tendency in rGO-Au composite because Au nanoparticle shows surface plasmon resonance absorption in visible region about 520 nm wavelength and inter-band excitation in ultra-violet region about 400 nm wavelength.

References

1. H. O. Pierson, *Handbook of Carbon, Diamond and fullerenes. Properties, Processing and Applications. brak miejsca: Noyes Publications,* (1993).
2. H. Marsh, et al., *Activated Carbon,* (1991).
3. J.N. Coleman, et al., *Science,* 331.6017 (2011) 568-571.
4. K.S. Novoselov, et al., *Nature,* 438.7065 (2005) 197-200.
5. K.S. Novoselov, et al., *Science,* 306.5696 (2004) 666-669.
6. L.M. Viculis, et al., *Science,* 299.5611 (2003) 1361.
7. Y. Hernandez, et al., *Nature Nanotechnology,* 3.9 (2008) 563-568.
8. X. Li, et al., *Science,* 324.5932 (2009) 1312-1314.
9. C. Berger, et al., *Science,* 312.5777 (2006) 1191-1196.
10. J. Cai, et al., *Nature,* 466.7305 (2010) 470-473.
11. Ž. Tomović, et al., *Angewandte chemie international edition,* 43.6 (2004) 755-758.
12. M. Treier, et al., *Nature Chemistry,* 3.1 (2011) 61-67.
13. S. Gilje, et al., *Nano Letters,* 7.11 (2007) 3394-3398.
14. S. Stankovich, et al., *Carbon,* 7.45 (2007) 1558-1565.
15. B.C. Brodie, *Philosophical Transactions of the Royal Society of London,*149 (1859) 249-259.
16. W.S. Hummers et al., *Journal of the American Chemical Society,* 80.6 (1958) 1339-1339.
17. D.C. Marcano, et al., *ACS Nano,* 4.8 (2010) 4806-4814.
18. W. Cai, et al., *Science,* 321.5897 (2008) 1815-1817.
19. W. Gao, et al., *Nature Chemistry,* 1.5 (2009) 403-408.
20. C. Mattevi, et al., *Advanced Functional Materials,* 19.16 (2009) 577-2583.
21. K. Erickson, et al., *Advanced Materials,* 22.40 (2010) 4467-4472.
22. A. Fasolino et al., *Nat. Mater.,* 6 (2007) 858.
23. C. Lee, et al., *Science,* 321 (2008) 385.
24. H. He et al., *Chem. Phys. Lett.,* 287 (1998) 53–56.
25. L. Staudenmaier et al., *Berichte der deutschen chemischen Gesellschaft,* 31.2 (1898) 1481-1487.
26. L. Staudenmaier et al., *Berichte der deutschen chemischen Gesellschaft,* 32.2 (1899) 1394-1399.
27. N.I. Kovtyukhova, et al., *Chemistry of Materials,* 11.3 (1999) 771-778.
28. J. Luo, et al., *Journal of the American Chemical Society,* 132.50 (2010) 17667-17669.
29. I.D. Rosca, et al., *Carbon,* 43.15 (2005) 3124-3131.
30. L. Becker, et al., *Proceedings of the National Academy of Sciences of the United States of America,* 97.7 (2000) 2979-2983.
31. J.A. McCleverty, *Nature,* 338.6211 (1989) 182-182.
32. K.R. Koch, *Journal of Chemical Education,* 59.11 (1952) 973.
33. A. Simon, et al., *Angewandte Chemie International Edition in English,* 26.2 (1987) 139-140.
34. A.L. Higginbotham, et al., *ACS Nano,* 4.4 (2010) 2059-2069.
35. F. Kim, et al., *Advanced Functional Materials,* 20.17 (2010) 2867-2873.
36. Ohtani B, et al., *Journal of Photochemistry & Photobiology, C: Photochemistry Reviews,* 11 (2010) 157–178 ISSN 1389-5567.

37. Fujishima A, et al., *Surface Science Reports*, 63 (2008) 515–582.
38. K. H. Wang, et al., *Applied Catalysis B,* 1 (1999) 21.
39. G. Darabdhara et.al., *Nanoscal*e, 8 (2016) 8276-8287.
40. https://www2.chemistry.msu.edu/faculty/reusch/VirtTxtJml/Spectrpy/UV-Vis/spectrum.htm#uv2.
41. T. Owen. *"Fundamentals of UV-visible spectroscopy (a primer)", Hewlett-Packard company, Germany*, 10 (1996).
42. L. Reimer, *"Scanning electron microscopy: physics of image formation and microanalysis", 2nd edition, Springer,* 1998.
43. E. Smith, et al., *"Modern Raman spectroscopy- a practical approach". John Wiley & Sons Ltd, England,* 1 (2005).
44. B.E. Warren, *X-ray Diffraction, General Publishing Company, (Classic x-ray physics book),* (1969).
45. *web.vu.lt/ff/m.vengris/images/TR_spectroscopy02.pdf*
46. M. Kim, et al., *KONA Powder and Particle Journal,* 10 (2016) 14356.
47. T. Asahi, et al., *Review of Scientific Instruments,* 69 (1998) 2.
48. K.H. Hung, et al., *Renewable Energy,* 66 (2014) 150-158.
49. H. Saleem, et al., *Materials Chemistry and Physics,* 204 (2018) 1-7.
50. K. Bramhaiah et al., *Advances in Nature Sciences: Nanoscience and Nanotechnology,* 3.045002 (2012) 6.
51. M. Nasrollahzadeh et al., *Journal of Colloid and Interface Science,* 466 (2016) 360-368.
52. F. Li, et al., *International Journal of Hydrogen energy,* 38 (2013) 14242-14249.
53. T. Smausz, et al., *Applied Physics A,* 123 (2017) 633.
54. P. Gnanaprakasam et. al., *Journal of Materials Chemistry A,* 3 (2015) 18010.
55. N. F. Atta et. al., *Analytical and Bioanalytical Chemistry,* 406 (2014) 6933-6942
56. J. E. Benedetti et. al., *RSC Advances,* 5 (2015) 33914-33922.
57. F. Kazemizadeh, et al., *Journal of Physics and Chemistry of Solids,* 104 (2017) 252-256.
58. M. Kanazawa, et al., *International Journal of Modern Physics B,* 32 (2018) 1840064.
59. Yamaguchi, et al., *International Journal of Modern Physics B,* 32 (2018) 1840073.
60. L.M. Malard, et al., *New Journal of Physics,* 15 (2013) 015009.
61. F. Carbone, et al., *Chemical Physics Letters,* 504 (2011) 37–40.
62. Md. Tariqul Islam et al., *New Journal of Chemistry,* 42 (2018) 8.

Research Activity

Academic paper

1. Yatin Madhukar Bhamare, Pankaj Koinkar, Akihiro Furube, M A More:
   Femtosecond Transient Absorption Spectroscopy of Laser-ablated Graphite and Reduced Graphene Oxide for Optical Switching Behavior, *Optical Materials: X 2 (2019) 100026*
   https://doi.org/10.1016/j.omx.2019.

Proceeding of International conference

1. Yatin Bhamare, Pankaj Koinkar, Akihiro Furube:
   Femtosecond Transient Absorption Spectroscopy of Graphite for Optical Switching Behavior,
   2018 International Conference on Physics and Mechanics of New Materials and Their Applications (PHENMA 2018), Busan, South Korea, Session B-2 Oral, 10 August 2018.

Proceeding of Domestic conference

1. Yatin Bhamare, Akihiro Furube, Pankaj Koinkar:
   Comparison of excited state dynamics between graphene and graphite using transient absorption spectroscopy,
   The Japan Society of Applied Physics Spring Meeting, Tokyo, 18p-P10-1 Poster, 18 March 2018.
2. Yatin Bhamare, Pankaj Koinkar, Akihiro Furube:
   Comparison of excited state dynamics of reduced graphene oxide decorated with Au, Pd, and Pt for photocatalytic degradation,
   The Japan Society of Applied Physics Spring Meeting, Tokyo, 11p-M112-10 Oral, 11 March 2019.

Attended conferences

1. *The Japan Society of Applied Physics Spring Meeting, Yokohama, Tokyo, 14-17 March 2017.*
2. *Materials Horizons Symposium: Electronic and Photonic Materials, Kyoto, 15 November 2017.*
3. *LED general forum, Tokushima, 12 February 2018.*
4. *Frontiers of Catalysis and Photo-Catalysis for Energy Chemistry, Kyoto, 25 January 2019.*